DISSERTATIONES
GEOGRAPHICAE
UNIVERSITATIS
TARTUENSIS
91

KALEV KOPPEL

Advancing urban and agricultural monitoring using Sentinel-1 synthetic aperture radar data

DISSERTATIONES GEOGRAPHICAE UNIVERSITATIS TARTUENSIS
91

DISSERTATIONES GEOGRAPHICAE UNIVERSITATIS TARTUENSIS
91

KALEV KOPPEL

Advancing urban and agricultural monitoring using Sentinel-1 synthetic aperture radar data

UNIVERSITY OF TARTU
Press
1632

Department of Geography, Institute of Ecology and Earth Sciences, Faculty of Science and Technology, University of Tartu, Estonia

This dissertation was accepted for the commencement of the degree of *Doctor philosophiae* in **geoinformatics** at the University of Tartu on March 10, 2025 by the Scientific Council of the Institute of Ecology and Earth Sciences at the University of Tartu.

Supervisor:

Prof. Tõnu Oja
Institute of Ecology and Earth Sciences
University of Tartu
Estonia

Opponent:

Prof. Ramon F. Hanssen
Department of Geoscience and Remote Sensing
Delft University of Technology
The Netherlands

Commencement:

Scientific Council Room in the University Main Building,
Ülikooli 18, Tartu, on May 5, 2025 at 12:15.

Publication of this thesis is granted by the Institute of Ecology and Earth Sciences, University of Tartu.

ISSN 1406-1295 (print)
ISBN 978-9916-27-847-5 (print)
ISSN 2806-2302 (pdf)
ISBN 978-9916-27-848-2 (pdf)

University of Tartu Press
www.tyk.ee

TABLE OF CONTENTS

LIST OF ORIGINAL PUBLICATIONS

This thesis is based on the following original publications which will be referred to in the text with their Roman numerals:

I Koppel, K., Zalite, K., Sisas, A., Voormansik, K., Praks, J., Noorma, M. (2015). Sentinel-1 for urban area monitoring – Analysing local-area statistics and interferometric coherence methods for buildings' detection. *2015 IEEE International Geoscience and Remote Sensing Symposium (IGARSS)*, 1175–1178. ©2015 IEEE.

II Koppel, K., Zalite, K., Voormansik, K., Jagdhuber, T. (2017). Sensitivity of Sentinel-1 backscatter to characteristics of buildings. *International Journal of Remote Sensing*, 38(22): 6298–6318.

III Voormansik, K., Zalite, K., Sünter, I., Tamm, T., Koppel, K., Verro, T., Brauns, A., Jakovels, D., Praks, J. (2020). Separability of Mowing and Ploughing Events on Short Temporal Baseline Sentinel-1 Coherence Time Series. *Remote Sensing*, 12(22), ARTN 3784.

The articles listed above have been printed with the permission of the copyright owners.

The articles are the result of collective work and contain an important contribution of all co-authors. The author's contribution to the publications referred to by their Roman numerals is indicated in the Table.

Table. Author's contribution to the publications (* – *minor contribution*, ** – *moderate contribution*, *** – *major contribution*).

	I	**II**	**III**
Original idea	***	***	*
Study design	***	***	*
Data collection	***	***	***
Analysis and interpretation	***	**	*
Manuscript writing	***	***	*

LIST OF ABBREVIATIONS

AI	artificial intelligence
ARIB	the Estonian Agricultural Registers and Information Board
az	azimuth
CAP	common agricultural policy
COH	interferometric coherence
DOY	day of year
ENL	equivalent number of looks
EO	earth observation
ESA	European Space Agency
EU	European Union
GIS	geographic information system
GRDH	ground range detected, high resolution; product level of Sentinel-1 images
gr rg	ground range
HH	horizontal transmit, horizontal receive
HV	horizontal receive, vertical transmit
InSAR	interferometric SAR
IW	interferometric wide swath mode
KDE	kernel density estimation
L2A	Sentinel-2 Level-2A product
LOS	line of sight
LoSSA	local spatial statistical analysis
ML	machine learning
MM	local area mean minus median
NASA	National Aeronautics and Space Administration
nDSM	LiDAR-based normalised digital surface model
NDVI	normalized difference vegetation index
NPA	national paying agency
POA	polarimetric orientation angle
PolSAR	polarimetric SAR
POP	buildings plan compactness ratio index
RON	relative orbit number
S1	Sentinel-1
S1A	Sentinel-1A
S1B	Sentinel-1B
S1C	Sentinel-1C
S1TBX	Sentinel-1 Toolbox software
S2	Sentinel-2
SAR	synthetic aperture radar
SD	speckle divergence
SLC	single look complex
SNAP	Sentinel application platform

SNR	signal-to-noise ratio
TAR	The Spatial Data Register of Tallinn
UN	United Nations
VH	vertical transmit, horizontal receive
VHR	very high resolution
VV	vertical transmit, vertical receive
γ	complex correlation coefficient (interferometric coherence)
σ^0	backscatter coefficient (backscatter intensity)

1. INTRODUCTION

1.1. Background

The next decades will bring further profound changes to the size and spatial distribution of the global population. The global urban population of 4.4 billion in 2023 is expected to double by 2050, at which point nearly seven of ten people will live in cities (World Bank, 2023). Cities play an increasingly important role in tackling climate change, because their exposure to climate and disaster risk increases as they grow. Cities are both victims of climate change and among its worst perpetrators: not only are they disproportionately exposed to its impacts, but they are also responsible for generating a large share of global emissions. Nevertheless, instead of concentrating on the negative aspects of urbanisation, cities should be seen as key players in achieving global climate goals. Compact cities with well-integrated transportation systems and energy-efficient buildings can be significantly more sustainable than suburban or rural areas (UN-HABITAT, 2024). With urban population growth and expansion expected to continue at unprecedented rates, accurate and timely monitoring of urban areas has become essential for effective planning, infrastructure development, and disaster management.

Hand in hand with increasing urbanisation and population pressure, fundamental food security problems are emerging: loss of agricultural land to expanding settlement, land degradation, low production productivity, and damaged environmental biodiversity. Agriculture and food security are also key sectors for intervention in the context of climate change (Vermeulen et al., 2012). Grasslands constitute 34% of the agricultural area used in the European Union (EU) (Eurostat, 2020), and play a significant role in livestock production, tourism, maintenance of biodiversity and protection against soil erosion (Hopkins and Holz, 2006). The protection of grasslands is one of the goals of the EU's Common Agricultural Policy (CAP), which encourages regular mowing and prohibits ploughing of permanent grasslands, while allowing it on agricultural grasslands. For landowners to receive financial support, grasslands must be maintained in good agricultural and environmental conditions. In Europe, monitoring of the mowing events is done by National Paying Agencies (NPA), who are responsible for verifying subsidy claims. Collecting evidence of the landowners' activities is time-consuming and costly as they are based on visual interpretation of high-resolution satellite images and a limited number of *on-site* inspections. Therefore, finding a cost-effective and accurate method is crucial to advance the verification of agricultural practices in large geographic areas. Furthermore, the growing number of satellite imagery providers gives an ideal opportunity to develop new methods and models using extensive time series of optical and radar imagery and more automated approaches for land monitoring.

Remote sensing is the acquisition of information about an object or phenomenon without making physical contact with the target in interest. In general usage, the term remote sensing refers to the use of satellite- or aircraft-based sensor technologies to detect objects on Earth. Monitoring and gaining versatile information about the widest possible area is the key to most of its applications. Remote sensing uses two types of methods: passive and active remote sensing. While passive sensors gather radiation that is emitted or reflected (e.g. sunlight) by the object, active collection emits energy to scan objects and areas, with a sensor (radar or lidar) then detecting and measuring the radiation reflected or backscattered from the target. Although radars have been used for the detection of ships and aircraft for almost 100 years, the breakthrough of constructing the Synthetic Aperture Radar (SAR) was made independently by Willey and Sherwin in the 1950s (Voormansik, 2014). SAR is an imaging radar capable of producing two-dimensional images of the Earth's surface. The first civilian spaceborne SAR satellite, Seasat, was launched by NASA in 1978. Seasat was followed by many successful SAR missions: e.g. SIR-A/B (1982/84), ERS-1/2 (1991/95), ALMAZ (1992), RADARSAT-1/2 (1995/2007), TerraSAR-X (2007), Tandem-X (2010), COSMO SkyMED (2010), ALOS-Palsar (2006), Sentinel-1A/ B/ C (2014/ 2016/ 2024).

SAR has many advantages compared to optical sensors. Radar carries its own source of illumination, making it independent of sunlight, and can penetrate cloud cover, allowing the collection of regular time series data about the dynamic phenomenon under study. The radar signal is also sensitive to the electrical and structural properties of the sensed objects. SAR polarimetry (polarimetric SAR or PolSAR) is a study of how the returns of differently polarised radar signals depend on the properties of the sensed object, i.e. structure, orientation, dielectric properties, and surface roughness. Another common application of SAR is interferometry (interferometric SAR or InSAR), where interferometry-based techniques are applied to make use of wave phase information from the backscattered radiation (Zalite, 2016). The InSAR technique uses two or more images of the same area acquired at different times and "interferes" (differences), resulting in maps called interferograms that show ground-surface displacement (range change) between the two time periods.

The Copernicus Sentinel-1 mission (S1) by the European Space Agency (ESA) was designed as a two-satellite constellation with frequent interferometric capability. The S1A was launched in 2014 and the S1B in 2016, but the latter ended its mission due to a technical malfunction in 2022. The S1C was launched on 5 December 2024 to replace the lost S1B (ESA, 2024a). S1 is well suited for urban and agricultural monitoring given frequent revisit times, close to all-weather capability, and a free data policy.

SAR is inherently well suited for the detection of urban areas from remotely sensed images as it is sensitive to the structure of the sensed object, including the dihedral and trihedral scatterers present in urban areas that generally cause a high backscatter. Detection of urban areas using SAR data is a relatively widely studied

topic. The approaches are varied, ranging from polarimetric analysis (Ainsworth et al., 2008; Cloude and Pottier, 1997; Moriyama et al., 2005) to interferometry (Gamba et al., 2000; Strozzi and Wegmuller, 1998).

However, most of the research has focused on the texture analysis of the intensity SAR data (Dekker, 2003; Dell'Acqua and Gamba, 2003; Tison et al., 2004). Approaches based on intensity are often preferred as they do not require additional pre-processing associated with interferometric or polarimetric methods. The intensity of backscatter has been used in several urban area retrieval methods, both as the only parameter and as one of several parameters (Bruzzone et al., 2004; Del Frate et al., 2008; Esch et al., 2010; Henderson, 1982). Intensity images of ERS-1, the first environmental monitoring satellite developed by ESA, were used in conjunction with other parameters to classify urban land cover classes in Del Frate et al. (2008) and carried the maximum information based on the relevance assessment. Similar findings based on multitemporal analysis of SAR data were also previously reported in a study by Bruzzone et al. (2004).

Backscatter information also plays a role in urban detection methods using more complex approaches also involving interferometric SAR (Chi et al., 2009; Liao et al., 2008; Strozzi and Wegmuller, 1998) or local area statistics and texture (Ban and Hu, 2007; Dell'Acqua and Gamba, 2006; Esch et al., 2010). Classification based on speckle analysis of the very high resolution (VHR) SAR TanDEM-X imagery has achieved high delineation accuracy (Esch et al., 2010, 2013). Approaches based on the fusion of SAR and optical data also rely on backscatter (Corbane et al., 2008; Houzelle and Giraudon, 1991).

Due to its dominant role in a multitude of urban detection methods, backscattering from buildings has been investigated and modelled in several studies: (Corbane et al., 2008; Dong et al., 1997; Kimura et al., 2005; Li et al., 2016; Quartulli and Datcu, 2004). As mentioned above, backscattering from urban areas is mainly dominated by specular reflections and is often analysed as a combination of three basic scattering mechanisms: single bounce from roofs; double bounce from wall-ground structures (dihedrals); and triple bounce from wall-wall-ground structures (trihedrals) (Dong et al., 1997). However, contributions from these structures vary with the orientation of urban objects to the sensor (azimuth and incidence angles), as well as polarizations, surface material, and roughness (Corbane et al., 2008; Kimura et al., 2005; Li et al., 2016). A comprehensive analytic evaluation of the return of a radar signal from an urban structure is presented in work by Franceschetti et al. (2002). Returns from this structure were evaluated on the basis of single, double, and triple scattering. Among other results, it was concluded that the sensitivity of the radar to the orientation of buildings depends on the angle of incidence and the roughness of the terrain.

Greater dependence was reported in case the incidence angle is larger than 30° and terrain roughness is low. Furthermore, it was shown that multiple scattering between walls and ground was dominant over a wide range of orientation angles when using co-polarised channel (VV – vertical transmit and vertical receive) and terrain roughness is small. For cross-polarised channels, multiple scattering was

always the dominant mechanism. Differences in returns from the HH (horizontal transmit and horizontal receive) and VH (vertical transmit and horizontal receive) channels were also reported in Dong et al. (1997). The differences were related to orientation, with a maximum HH response recorded for orientation angles smaller than 10°, while for VH backscatter the maximum occurred at 45° orientation.

Remote sensing of grasslands is a widely studied topic. Although optical remote sensing of grasslands offers a wide range of techniques, it suffers from the limited availability of regular and timely acquisitions during the growing season due to cloud cover. It especially harms methods that rely on time series analysis to measure temporal differences caused by plant phenology and management practices. SAR data is considered an effective solution for monitoring agricultural activities, providing continuous data while covering extensive areas (McNairn and et al., 2009). Although SAR data might not completely substitute optical data, it is a valuable supplement in combination. In recent years, the number of studies that consider optical and SAR time series data for grassland mowing detection has increased (Erasmi and Twele, 2009; Hill and et al., 2005; Lobert et al., 2021; Reinermann et al., 2022).

S1 is able to produce coherence maps on a wide scale with weekly intervals (depending on how many satellites are on the orbit). Attempts to relate coherence to mowing and ploughing events on grassland are relatively recent, but are based on well-established studies. Changes in the placement of the scatterer in the soil and the canopy lead to a loss of coherence over time (Hagberg et al., 1995; Zebker and Villasenor, 1992). Low coherence can be an indication of the presence of vegetation or farming activity, and high coherence can indicate sparse vegetation or lack of it due to e.g. mowing (Wegmuller and Werner, 1997). However, change due to wind and precipitation causes coherence to decrease over time (Askne et al., 2003; Hagberg et al., 1995; Lavalle et al., 2012; Santoro et al., 2010), making the interpretation ambiguous.

As earlier studies show, short vegetation after mowing results in high coherence in the case of COSMO-Skymed interferometric pairs with a one-day temporal baseline (Zalite et al., 2016). A similar effect is present on TerraSAR-X Staring Spotlight coherence images with a temporal baseline of 11 days (Ali et al., 2017). A comprehensive effort to relate S1 12-day coherence with mowing events in Tamm et al. (2016) demonstrated the value of S1 coherence for agricultural applications.

Today, the triumph of artificial intelligence (AI) and machine learning (ML) significantly affects scientific research, including the development of remote sensing methods. Traditional research of remote sensing data and deep domain knowledge in e.g. SAR physics, respectively, is irreplaceable in the feature engineering process to prepare high-quality input features for the training of ML algorithms. Advanced ML algorithms are well suited for complex data fusion, time series analysis and automated pattern recognition. The application of artificial neural networks to the second-order S1 backscatter time series has shown reasonable accuracy for grassland mowing detection (Taravat et al., 2019).

In another research, grassland mowing events have been studied by modelling NDVI on a parcel level with recurrent neural networks using S1 backscatter and coherence time series as input features (Garioud et al., 2020). Komisarenko et al. (2022) used convolutional neural networks for mowing detection based on the time series of S1 and S2. The proposed model significantly outperformed the state-of-the-art technique and achieved an event detection accuracy of 73.3% and an end-of-season accuracy of 94.8%.

1.2. Objectives and progress of this work

This thesis focuses on harnessing remote sensing data, particularly from the ESA Copernicus S1 SAR mission, to address two primary applications: (1) monitoring urban areas to detect built-up structures and analyse how the main characteristics of the building impact backscatter values, and (2) identifying and classifying mowing and ploughing events on agricultural land to support the EU's CAP compliance monitoring and broader land use applications. In this thesis, both PolSAR and InSAR methods, e.g. interferometric coherence, are used and studied. The axis of this work is method development for the implementation of potential monitoring applications based on S1 data. The objects under study, for example urban areas, specific buildings, or grassland mowing events, vary in their temporal dynamics and spatial scale.

The main objectives of this thesis are:

1. Investigating methods based on local area statistics from S1 imagery for built-up area detection (**I**).
2. Exploring how different physical parameters of buildings influence the radar backscatter detected by S1 SAR. The key factors analysed are building height, alignment, regional density, shape, and wall material, as these attributes can affect backscatter strength and clarity in SAR imaging (**II**).
3. Distinguishing between mowing and ploughing activities in grasslands based on analysis of SAR interferometric coherence and NDVI time series data (**III**).

Under normal conditions, physical change in the urban environment is a relatively slow and gradual process, which does not assume excessive or unnecessary effort in processing long and continuous time series with fine temporal resolution. Instead, it is more effective to generate accurate snapshots in time based on a representative number of acquisitions for proper signal processing. The study in **I** evaluates techniques for detecting built-up areas using S1A SAR imagery. The study explores three specific methods: (1) Mean-Median (MM), (2) Speckle Divergence (SD), and (3) Interferometric Coherence (COH). This study introduces and develops a novel, computationally efficient yet accurate method for detecting built-up areas from SAR imagery.

The next essential step was to understand how the S1 backscatter values are affected by the physical characteristics of buildings to discover possible limita-

tions that could be used to further improve current backscatter-based built-up area detection methods. The study in **II** presents the quantitative analysis how key factors such as building height, alignment to the SAR sensor, regional density, building shape, and wall material can affect backscatter strength and clarity in SAR imaging. This study leverages a comprehensive building database to provide empirical evidence supporting SAR theory while identifying its practical limitations in real-world applications.

To study and demonstrate the application of S1 SAR data in more dynamic settings, another complex environment – grassland – was selected. The study in **III** investigates the ability to detect agricultural activities, specifically mowing and ploughing, using S1 SAR coherence time series data. This capability is essential to monitor grassland management under the EU CAP. This study characterises the dynamics of S1's 6-day coherence time series, since S1B data were newly available, with respect to mowing and ploughing events on agricultural grasslands in Estonia. S1 coherence time series of more than a thousand grassland parcels were aggregated and analysed in relation to recorded agricultural management events. To the best of the authors' knowledge, this is the first study that includes such a large set of ground reference data, providing significant value for conclusions and generalisations. The results support the use of SAR coherence time series for CAP compliance and have potential applications in food security and land use monitoring.

The practical motivation for this study is the development of an operational service by the Earth observation company KappaZeta Ltd. to support the Estonian Agricultural Registers and Information Board (ARIB) in monitoring compliance with EU CAP requirements for grassland management.

2. MATERIALS AND METHODS

2.1. Study sites

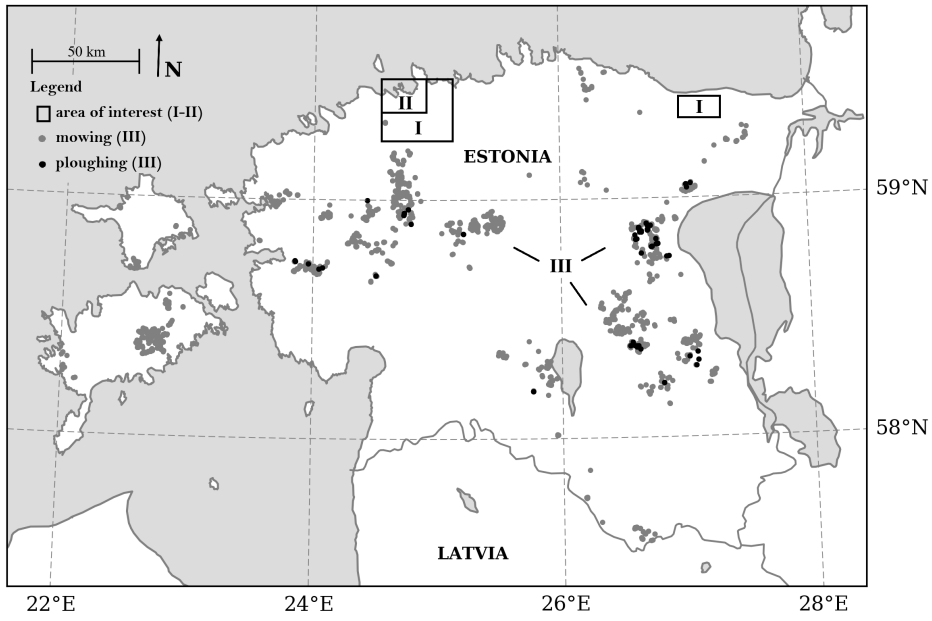

Figure 1. Location of the study areas in Estonia. Roman numerals refer to Publications. In case of Publication **III** the size of markers is not to scale. Source: adopted from Publication **III** Figure 1.

The study areas for urban detection (**I**) were selected due to different dynamics of population and settlement, as well as the availability of detailed digital data on building stock for the analysis of SAR sensitivity (**II**) (Figure 1).

Tallinn and its surrounding areas in Harju county are among the fastest growing regions in Estonia. The population of Tallinn city on January 1, 2014 was ∼411 000, while for the whole Harju county, the number was ∼572 000. Ida-Viru, an industrial area in the north-east of the country, includes the mining towns of Kiviõli, Püssi and Kohtla-Järve, and represents a region with rapid population decline and abandoned residential areas in the scenery of a heavy industrial landscape. The Ida-Viru county had a permanent population of ∼149 000 (Statistics Estonia, 2024).

The grasslands used for detecting agricultural activities (**III**) are geographically evenly distributed across Estonia, ensuring a representative dataset for the development of a nationwide monitoring application.

2.2. Reference data

2.2.1. Reference data for built-up areas

To compare different built-up area detection methods in the study **I** reference data for land cover classes were obtained from the Estonian Land Board's Topographic Database (Estonian Land Board, 2024). Two land cover classes were defined: (a) built-up areas and (b) non-built-up areas. To account for the ground resolution of the S1A data, a 20-meter buffer was added to the building polygons. The remaining pixels within the area of interest (encompassing the reference data on buildings) were assigned to the non-built-up class.

2.2.2. Reference data for building parameters

To analyse how different physical parameters of buildings influence the radar backscatter detected by S1 in the study **II** a database of building attributes was created using two primary data sources:

1. The Spatial Data Register of Tallinn (TAR) – containing 2D building contours at a scale of 1:2000 and descriptive information for 51 599 buildings as of December 9, 2015.
2. LiDAR-based normalised digital surface model (nDSM) from the Estonian Land Board, with data collected in 2013.

The following attributes were calculated for each building:

1. Mean building height, extracted from the nDSM model (1×1 m pixel size).
2. Alignment of the main axis of the building polygon relative to the S1 orbit.
3. Main wall material, sourced from TAR.
4. Regional density, expressed as the volume within a 100×100 m grid cell (m^3ha^{-1}).
5. Compactness of the building's external shape, calculated using the plan compactness ratio (POP) index (Equation 2.1).

Tallinn, with an administrative area of 159 km^2, is divided into eight administrative units. The study area encompasses a variety of urban and architectural features, including medieval stone buildings in the Old Town, modern glass and steel towers in the City Centre, and heavy industrial zones in Northern Tallinn and the Lasnamäe district. It also includes low-density residential districts with dense tree canopies, such as Nõmme and Pirita. Residential housing in Lasnamäe, Mustamäe, and Õismäe (located in the Haabersti district) consists primarily of panel block apartment buildings, ranging from 5 to 16 stories, constructed during the 1970s–1990s.

The heights of Tallinn buildings are uneven due to city planning regulations, with peaks at 7 m, 17 m, and 27 m, corresponding to two, five, and seven-story buildings, respectively (Figure 2(a)). Most buildings (66%) are one- or two-storey, averaging below 7 m in height. Buildings with heights below 2 m were excluded

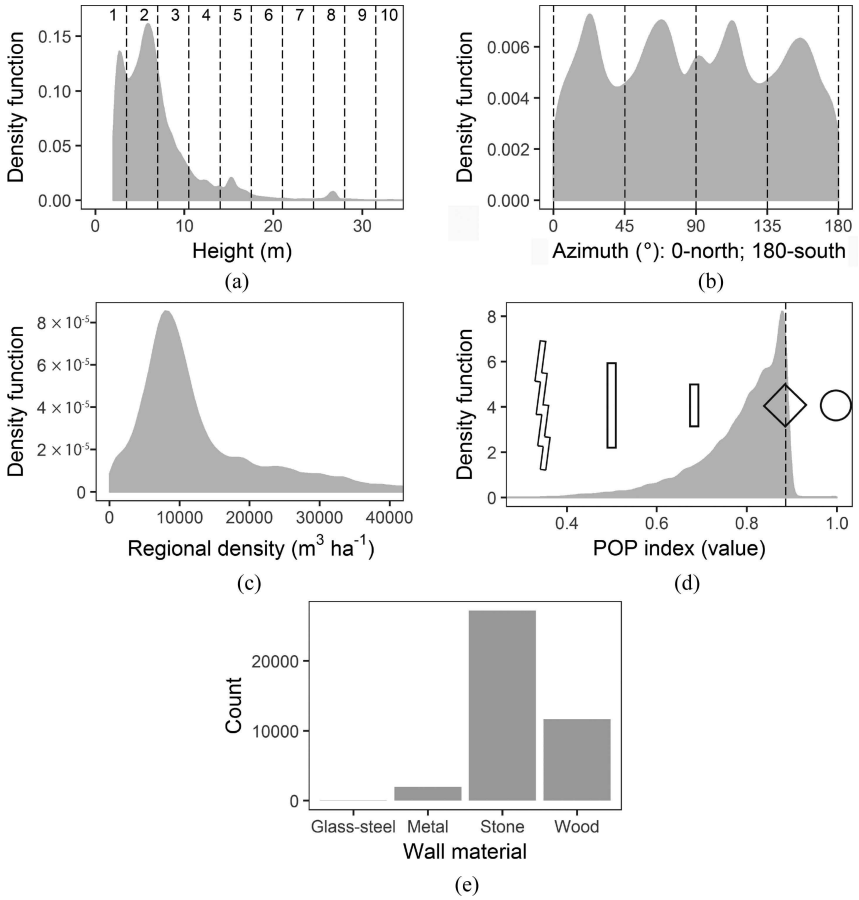

Figure 2. Characteristics of the building stock: (*a*) density function (KDE) of the height with approximate number of storeys indicated by vertical lines; (*b*) density function of orientation with respect to north; (*c*) density function of regional density; (*d*) density function of POP index with respective indicative shapes plotted over; (*e*) count by material (category "Glass-steel" contains 23 buildings). Source: Publication **II** Figure 5.

from the final dataset, as their measurements were often distorted by neighboring tree canopies extending over their roofs.

To determine the alignment of the buildings to the S1 orbit, the azimuth values of the longer axis of the input polygon features were calculated. The azimuth was measured clockwise, starting from 0° at the top/north to 180° at the bottom/south. These angles were then adjusted to account for the heading azimuth of the satellite platform for both ascending (az 342.35°) and descending orbits (az 197.63°). The orientation of the buildings in Tallinn is irregular, with peaks around ±20° and ±70°, reflecting the right-angle street networks aligned with the transport routes and the coastline (Figure 2(*b*)).

The regional building density was calculated using a 100 m×100 m grid (fishnet). The total building volume in m^3 within each grid cell was calculated

and then attributed back to the individual buildings located within that cell. The most densely built areas include Northern Tallinn, the City Centre, Lasnamäe, Mustamäe, and Õismäe. However, 51% of buildings are in low-to-moderate density regions (<10 000 $m^3 ha^{-1}$, Figure 2(*c*)).

The compactness of a building's external shape is represented by the POP index (Brandon, 1977). This method uses a circular shape as the reference point, as a circle has the smallest ratio between circumference and area, resulting in a POP index of one. The POP index decreases as the complexity of the shape increases. The POP index is defined as follows:

$$\mathrm{POP} = \frac{2\sqrt{\pi A}}{L} \tag{2.1}$$

where: POP – the plan compactness ratio index, L – the perimeter of a building calculated from the contour of the outer walls, and A – the surface area of the building's projection.

This method does not consider the shape of the roof, as such data is unavailable in the TAR. In addition, the roof material is not recorded. However, the register provides information about the primary material of the building's walls, categorised into four classes: stone, wood, metal, and glass and steel. Most buildings in Tallinn have rectangular floorplans, with POP index values greater than 0.886 indicating compact shapes. About 2% (897) are circular and 1. 7% (731) have highly complex floorplans (POP < 0.5). However, the POP index may underestimate true 3D complexity (Figure 2(*d*)).

Tallinn's buildings are mainly made of stone (66.5%) or wood (28.6%). Less common materials include metal (4.8%) and glass/steel (0.1%; 23 buildings, Figure 2(*e*)).

2.2.3. Reference data for agricultural events

In the study **III** data on management events were collected directly from Estonian farmers: 1695 mowing and 195 ploughing events on 1159 and 177 unique agricultural parcels, with an average area of 10.4 ha (range: 0.6–108.5 ha) for mowing, and 12.2 ha (range: 0.9–92.0 ha) for ploughing. The mowing occurred from May 20 to October 12, 2017, while the ploughing spanned July 1 to September 8, 2017. The events were geographically evenly distributed throughout Estonia (Figure 1).

As the SAR signal is sensitive to water and precipitation causes variations in relative permittivity in the resolution cell, the local weather and precipitation data were derived from the Estonian Weather Service database (Estonian Weather Service, 2024).

Table 1. Parameters of the SAR data used in studies **I–II**. Asterisk denotes the images used in the study **II**. In the last row is the mean incidence angle for the area of interest. Source: adopted from Publication **I** Table 1.

Date	Orbit	Prod. Type	Area	Inc. angle
2015.03.02	ASC	SLC	Tallinn	42°
2015.03.09	ASC	GRDH	Ida-Viru	42°
2015.03.11	DESC	GRDH	Ida-Viru	44°
2015.03.26	ASC	SLC	Tallinn	42°
2015.03.28*	DESC	GRDH	Tallinn	45°
2015.03.28	DESC	SLC	Tallinn	45°
2015.03.28	DESC	SLC	Ida-Viru	38°
2015.04.02	ASC	SLC	Ida-Viru	42°
2015.04.07*	ASC	GRDH	Tallinn	42°
2015.04.21	DESC	SLC	Tallinn	45°
2015.04.21	DESC	SLC	Ida-Viru	38°
2015.04.26	ASC	SLC	Ida-Viru	42°

2.3. Satellite data

The SAR data for this thesis were collected by the ESA's Copernicus programme's Sentinel-1 (S1) satellite mission employing a constellation of two identical satellites (then A and B, now A and C units) in the shared Sun-synchronous orbit. The Sentinel-1A (S1A) and Sentinel-1B (S1B) satellites use $\sim$ 5.6 cm wavelength microwaves (C-band) for imaging.

In the study **I** ten acquisitions were used: six in the Single Look Complex (SLC) format to analyse repeat pass interferometric coherence and four in the Ground Range Detected High Resolution (GRDH) format to analyse local statistics (Table 1). To investigate the effects of different look directions and polarisation combinations both the VV (vertical transmit, vertical receive) and VH (vertical transmit, horizontal receive) channels of images acquired from ascending and descending orbits were included. For the SAR sensitivity analysis in the study **II** two S1 acquisitions in GRDH format were used: one from a descending orbit (2015.03.28) and another from an ascending orbit (2015.04.07), providing two independent observations from different viewing directions.

Each satellite in the S1 constellation returns to the exact same orbital position every 12 days, whereas the combined re-visit cycle of the two satellites is 6 days allowing to form dense and continuous time series over the test sites. For the coherence time series analysis in study **III** a total of 386 S1A/B SLC IW products, acquired between May 1 and October 30, 2017, were processed, with overpass times around 18:00. These included 87 products from the relative orbit number (RON) 160, 62 from RON 131, 84 from RON 87, 93 from RON 58, and 60 from RON 29, organised into S1A/S1B 6-day pairs. Only nine products were missing during this period, slightly reducing the data density for RON 160 and

RON 87. Incidence angles range between 29° and 46°. The spatial resolution ranges between 2.7 m and 3.5 m in slant range but is fixed at 22 m in azimuth.

In the study **III** also the optical remote sensing data from the ESA Copernicus Sentinel-2 (S2) mission were used. 351 S2A/B L2A products, acquired in the same time frame, were processed, with overpass times around 13:00. These comprised 14 products from RON 22, 74 from RON 36, 67 from RON 79, 50 from RON 93, 78 from RON 122, and 68 from RON 136. For S2, only the Normalised Difference Vegetation Index (NDVI) time series were calculated to provide a comparison with the optical vegetation remote sensing parameter, since the focus was on the S1 coherence analysis.

2.4. Methods based on local statistics

Local spatial methods in the field of geoinformatics examine the characteristics of spatial subsets (local spaces) defined with respect to a complete data set (global space). Such methods have evolved independently in the fields of geography, GIS, cartography, remote sensing, and landscape ecology (Boots and Okabe, 2007). The spatial subset or local area of interest can be defined using a kernel (e.g., rectangular, circular) centred on and surrounding the point of interest (e.g., a single pixel) or by a polygon (e.g., vector mask, image segment) representing the area (Tamm, 2018). In this study, the term *local area statistics* is defined as statistical measures calculated within the local area of interest from a remotely sensed image. Local spatial statistical analysis (LoSSA) encompasses the nature of spatial subsets, their spatial relationship to the complete data set, and the relationship between a given global statistic and the corresponding local statistics computed for the data set (Boots and Okabe, 2007).

In this thesis, three local area statistics (Section 2.4.1–2.4.3) were evaluated in terms of their precision to delineate urban areas from the S1A images (**I**) and one of them – the interferometric coherence – was applied to detect agricultural events from the S1A and S1B time series (**III**). Statistical analysis based on the arithmetic mean of the SAR backscatter values under the building polygon as a local area of interest (**II**) belongs to the same methodological approach.

2.4.1. Local area mean minus median

The local area mean minus median (MM) makes the assumption that the skewness of the distribution of the backscattering coefficient for different land use classes varies. When the distribution of backscattering values of the natural targets is Chi (normal), then for the urban targets it is more skewed and asymmetric. Additionally, the MM values take into account the backscatter amplitude, which is not normalised. Thus, it would be possible to exploit not only the differences in the values' distributions but also the inherently more powerful backscattering from artificial targets.

Classically, skewness is computed as follows:

$$\text{skew} = \frac{\sum_{i,j}(x_{ij} - \bar{x})^3}{(n-1)\sigma^3} \tag{2.2}$$

where x_{ij} stands for the value of a pixel at position (i, j) in the kernel, n is the number of pixels in the kernel and σ is the standard deviation of the values in the kernel. According to the MM method, the median value of the pixels inside the kernel is subtracted from their mean value:

$$MM = \langle \bar{S} \rangle_{xy} - \langle \tilde{S} \rangle_{xy} \tag{2.3}$$

where $\langle \ldots \rangle_{xy}$ denotes the set of σ^0 values inside a kernel of size $x \times y$, $\bar{S}$ denotes the mean value and $\tilde{S}$ denotes the median value.

SAR backscatter is orientation-dependent. To minimise this dependence, an analysis should be performed on two acquisitions: one from an ascending path S_{asc} and one from a descending one S_{desc}. The maximum value of the two MM images $max(S_{asc}, S_{desc})$ is then assigned to a pixel in the output image.

2.4.2. Speckle divergence analysis

Speckle divergence analysis (SD) is a local statistics method that is based on speckle noise reduction and the texture analysis of SAR images. Local speckle characteristics provide a texture layer that highlights built-up areas. Regarding the local deviation from the fully developed speckle, speckle divergence increases with a rising amount of true structures within the resolution cell. The variation of structures leads to local heterogeneity that gives urban areas a very specific and distinct appearance in SAR images (ESA, 2024c).

Thiel et al. (2008) and Esch et al. (2010) developed SD to detect the settlement area using TerraSAR-X. They achieved more appropriate noise suppression compared to established filtering routines, which preserve true structures with texture and contour information. This filter was based on the sigma probability of the Gaussian distribution of speckle noise. It removes speckle and suppresses noise, but preserves texture, structure, and contour information. This was indispensable since many regions were characterised by small-scale structures (Khomarudin and Indrajit, 2012).

The calculation of speckle divergence was based on a kernel size of 9×9 pixels, and the formulas were stated as follows:

$$D_{x,y} = C_{x,y} - C \; with \; C_{x,y} = \frac{\sigma_{x,y}}{\mu_{x,y}} \tag{2.4}$$

where $D_{x,y}$ denotes the speckle divergence, C denotes the theoretical heterogeneity due to developed speckle, it was calculated from the inverse of the equivalent

number of looks (ENL), $ENL = L_a + L_r = 1/C$; L_a and L_r defining the effective number of looks in the azimuth and range (stated in TerraSAR X metadata), $C_{x,y}$ denotes the local coefficient of variation, calculated in a kernel size of 9×9 pixels, $\sigma_{x,y}$ denotes the local standard deviation, calculated in a kernel size of 9×9 pixels, and $\mu_{x,y}$ denotes the local mean, calculated in a kernel size of 9×9 pixels. In the study **I** a kernel size of 5×5 pixels was used due to a lower spectral resolution.

2.4.3. Interferometric coherence

Interferometric coherence (COH) can be used to detect changes in the observed target area over the time between two acquisitions. Natural targets tend to lose coherence faster than non-natural targets, leading to the use of the coherence parameter to detect built-up areas (Strozzi and Wegmuller, 1998). The amplitude of the complex correlation coefficient (i.e. coherence) is calculated for two complex SAR acquisitions s_1 and s_2 as

$$\gamma = \frac{|\langle s_1 s_2^* \rangle|}{\sqrt{\langle s_1 s_1^* \rangle \langle s_2 s_2^* \rangle}}, \quad 0 \leq \gamma \leq 1. \tag{2.5}$$

The estimated coherence γ is the product of several terms specific to the measurement system, the data processing steps, and the targets that were imaged. It can be modelled as follows:

$$\gamma = \gamma_t \gamma_n \gamma_{others}, \tag{2.6}$$

where γ_t refers to temporal decorrelation, γ_n refers to decorrelation due to signal-to-noise ratio, and γ_{others} refers to other terms that may be present but can be considered as negligible in our case (Hanssen, 2001).

According to (Morishita and Hanssen, 2015; Rocca, 2007; Zebker and Villasenor, 1992), γ_t can be expressed as

$$\gamma_t = e^{-t/\tau}, \quad \text{with} \tag{2.7}$$

$$\tau = \frac{2}{\sigma_r^2} \left(\frac{\lambda}{4\pi} \right)^2, \tag{2.8}$$

where t is the temporal baseline between acquisitions, λ is the radar wavelength, and σ_r is the mean motion of the scatters in the line of sight (LOS). γ_t is a measure of change over time; it approaches 1 in case σ_r approaches 0.

2.4.4. Interpretation of coherence time series for grasslands monitoring

In the case of the management of agricultural grasslands (**III**), there are three distinct phases which we need to evaluate in relation to γ: growth, the mowing or ploughing event, and the developed state. Growth occurs in the early vegetation season and after events. The developed state occurs between the previous states when the vegetation is steady and relatively tall.

The movement and growth of vegetation in the line of sight (LOS) causes temporal decorrelation. Coherence also decreases due to variations in soil and vegetation moisture content, which affects the location of the scattering centre, as seen by SAR. During the growth phase, the physical and moisture changes are gradual. Changes accumulate as more vegetation is visible in the LOS causing decorrelation. Coherence would remain low throughout the developed phase.

The removal of vegetation during a mowing event acts in two ways in relation to γ_t. The actual event drastically changes the scatterers. γ_t calculated for an image pair where the event occurred between the acquisitions would be very low. Depending on the canopy cover, it can be even lower than the coherence of the developed state. For image pairs after the actual event, γ_t would be higher compared to pairs where vegetation was present – as the vegetation is removed, the returns from more coherent soil increase.

Similar behaviour applies to ploughing. The event itself causes decorrelation, and the conditions after it would cause a higher γ_t. The total lack of vegetation would suggest even higher γ_t values than in the case of mowing.

Precipitation is a source of decorrelation. Variations in relative permittivity in the resolution cell between acquisitions cause coherence to decrease, as the scattering centre changes according to permittivity change. Variations are difficult to predict as one must consider a multitude of factors, including air temperature, wind, soil, and vegetation conditions.

The estimated γ is also a function of Equivalent Number of Looks (ENL) defined by the size of the averaging window in Equation 2.5 (Lee et al., 1994). The contrast between areas of low coherence will be lost if a small averaging window (resulting in low ENL) is used in Equation 2.5 (Touzi et al., 1999). I used an averaging window that ensures a square footprint on the ground (approx. 70 m $\times$ 70 m) and an ENL value between 40 and 50, depending on the swath. According to (Cumming and Wong, 2005; Lee et al., 1994), ENL of 45 would ensure contrast for γ values larger than 0.13. Correction for γ_n term in Equation 2.5 was applied according to (Just and Bamler, 1994).

2.5. SAR data processing and analysis

Depending on the objective and respective methods different SAR data processing steps were applied to prepare the SAR data for the analysis. SAR data processing was performed using Sentinel-1 Toolbox (S1TBX) software (ESA, 2024b) in the study **I** and the Sentinel Application Platform (SNAP) 2.0 in studies **II**–**III**. The

detailed technical description of pre- and post-processing steps of the SAR data is described in the respective publications and not repeated here.

For built-up area detection in the study **I** the local area statistics – including arithmetic mean, median, speckle divergence and coherence – were calculated using a 5×5 pixel kernel as it provided the best results with 10 m pixel resolution, while larger kernels produced overgeneralised map patterns. Using the reference data, histograms were computed for built-up and non-built-up areas for each method (MM, SD, COH). The 95th percentile of the values representing non-urban areas was selected as the threshold value. This threshold was then used to classify the image pixels into two classes, built-up and non-built-up, using a threshold-based classification approach. Finally, the total classification accuracy and the user's accuracy were calculated from the confusion matrix.

For the analysis of SAR sensitivity to building parameters in the study **II** only two S1 acquisitions in GRDH format were used: one from a descending orbit and another from an ascending orbit to provide two independent observations from different viewing directions. VH and VV polarisation backscatter images from both orbits were exported in GeoTIFF format for further processing in GIS software. Buffering around individual buildings was applied to mitigate distortions in SAR backscatter values caused by overlay and shadow effects in densely built-up areas. For each building, a buffer zone was calculated based on its height and the steepest incident angle (40.80°) within the study area: height × 1.16. The SAR backscatter images, originally at 10 m pixel resolution, were resampled to 1 m pixel resolution. The mean backscatter values for the building polygons were calculated and the mean linear σ^0 values were converted to the dB scale. The mean backscatter values for the VH and VV polarisation bands were calculated for each building in the database. Data from ascending and descending orbits were treated as two independent observations of the same objects (e.g. buildings). The mean backscatter values from the two orbits were merged into common attribute fields for each polarisation band, doubling the number of database entries to 81 810. Since mean backscatter values from the ascending orbit were higher due to the steeper incident angle, they were fitted by subtracting the observed differences: 1.32 dB for VH and 1.10 dB for VV polarisation. Statistical analysis and data visualisation were performed using the R software environment. First, the distribution of backscatter was analysed with respect to each parameter to interpret its influence on backscatter values. Then a correlation matrix was computed for all physical parameters and backscatter values to evaluate their statistical relationships.

For agricultural events detection on grasslands in the study **III**, the coherence was calculated separately for each swath. Then SAR data was resampled to a 4-m resolution to maintain the maximum spatial resolution while ensuring square-shaped pixels. To ensure accuracy, only pixels entirely within the parcel boundaries (accounting for the averaging window used in the coherence calculation) were included in the results, eliminating interference beyond the parcel borders. To analyse how γ varies in relation to mowing and ploughing events, γ

values from all parcels with recorded events were aggregated. All time series were aligned to a common grid with a one-day step, centering the event at time 0. The grid spans from -30 days (i.e., 30 days before the event) to $+30$ days. For each grid point, the median, as well as the first and third quartiles, were calculated. The ploughing signatures are shown within a limited range of -10 to $+30$ days, since the condition of the grasslands prior to ploughing was too variable to allow meaningful generalisation.

3. RESULTS

3.1. Local area statistics for built-up area detection

In the study **I** the total accuracy and the user's accuracy[1] were calculated for each of the 24 classified images, which represent the pair-wise combinations of two study areas (Tallinn and Ida-Viru), three methods (SD, MM, and COH), two orbits (ascending and descending), and two polarisations (VV and VH) (Table 2).

In general, the user's accuracy is lower for Ida-Viru compared to the Tallinn area. The results of the ascending and descending orbits are similar. The COH method appears to perform consistently across all combinations of orbit and polarisation. For SD and MM methods, the classification accuracies for the VV channel are higher than those for the VH channel. This indicates that most of the reference buildings are orientated perpendicular to or nearly perpendicular to the satellite's look angle. Strong VH backscatter from buildings is observed when they are orientated at 45° relative to the satellite flight path. Additionally, a strong response in the VV channel suggests surface backscattering from the roofs.

Higher accuracies are achieved for all methods when the results from VV and VH channels are combined using the logical OR operator (Table 3). Furthermore, combining not only polarizations but also orbits yields the highest accuracy.

In general, the MM method achieved the highest accuracy for Tallinn (72%, combining both orbits and polarisations), while the SD method performed best for Ida-Viru (57%, combining both orbits and polarisations). Although the SD method delivered high accuracy, it suffered from over-classification due to an edge detection effect: features such as roads, riverbanks, and lake edges were incorrectly classified as built-up areas. This issue was less pronounced for the MM method, which incorporates the amplitude of the backscatter because the magnitude of the backscatter from these features is generally lower than that from built-up areas.

For both MM and SD methods, the optimal kernel size for S1A interferometric wide swath mode (IW) images with a 10×10 m pixel resolution was found to be 5×5 pixels. Larger kernel sizes (e.g., 7×7 and 9×9 pixels) caused additional features, such as forest edges and cliffs, to be misclassified as built-up areas.

All methods demonstrated higher accuracy for the Tallinn study area, likely because built-up areas in Ida-Viru are more rural and therefore more vegetated. Similarly, within Tallinn, areas with greater vegetation coverage were classified with lower accuracy.

[1]The urser's accuracy represents class-wise accuracies from the point of view of the map user. The user's accuracy is calculated by dividing the number correctly classified samples of class c by the number of samples classified as class c. It therefore provides the map user with a probability that a particular map location of class c is also the same class c in truth (Humboldt-Universität, 2024).

Table 2. Assessment of detection of built-up areas with SD, MM and COH methods for individual scenes. Legend: total accuracy %/ user's accuracy % (for built-up areas). Source: Publication **I** Table 2.

		Asc. orbit		Desc. orbit	
	Method	**VV**	**VH**	**VV**	**VH**
Tallinn	**SD**	90 / 37	89 / 27	90 / 38	89 / 28
	MM	90 / 36	89 / 19	90 / 27	89 / 21
	COH	85 / 35	85 / 36	84 / 31	84 / 33
I.-Viru	**SD**	92 / 27	91 / 16	92 / 35	91 / 19
	MM	92 / 33	91 / 20	92 / 34	91 / 21
	COH	88 / 14	88 / 13	88 / 18	88 / 13

Table 3. Assessment of detection of built-up areas with SD, MM and COH methods for combinations of scenes. Legend: total accuracy %/ user's accuracy % (for built-up areas). Source: Publication **I** Table 3.

		ASC	DESC	ALL
	Method	**VV+VH**	**VV+VH**	**combined**
Tallinn	**SD**	89 / 48	89 / 49	88 / 68
	MM	90 / 50	91 / 43	89 / 72
	COH	85 / 56	83 / 46	81 / 53
I.-Viru	**SD**	91 / 36	91 / 39	89 / 57
	MM	92 / 32	92 / 34	91 / 54
	COH	78 / 38	82 / 35	70 / 56

3.2. Sensitivity of SAR backscatter to building parameters

3.2.1. Backscatter vs physical parameters

To assess how building parameters influence S1 backscatter in the study **II**, the distribution of each parameter was plotted as a function for continuous variables (height, alignment, regional density, POP index) and as a boxplot for the discrete variable (material) (Figure 3). For both VH and VV channels, the mean backscatter values (thick line), 95% confidence intervals (grey area), and 0.25/0.75 quantiles (thin lines) were plotted. The function lines were smoothed with a generalised additive model (GAM) procedure that is an automated fitting and smoothing technique invented by Hastie and Tibshirani (Hastie and Tibshirani, 1990).

Building height significantly affects backscatter in both channels. The backscatter of buildings taller than 20 m is approximately 9 dB stronger than from those under 3.5 m (Figure3(a)), with mean values increasing steadily with height. The dihedral and trihedral focus the backscatter to the same point on a radar image (Auer and Bamler, 2010). The larger wall surface returns a brighter signal. However, deviations occur for very tall buildings (>20 m). There may be several reasons: (1) structures like industrial chimneys and communication towers that are lacking walls, produce weaker backscatter; (2) the side-looking SAR with incidence angles (41–46°), create overlay effect where returns from building tops

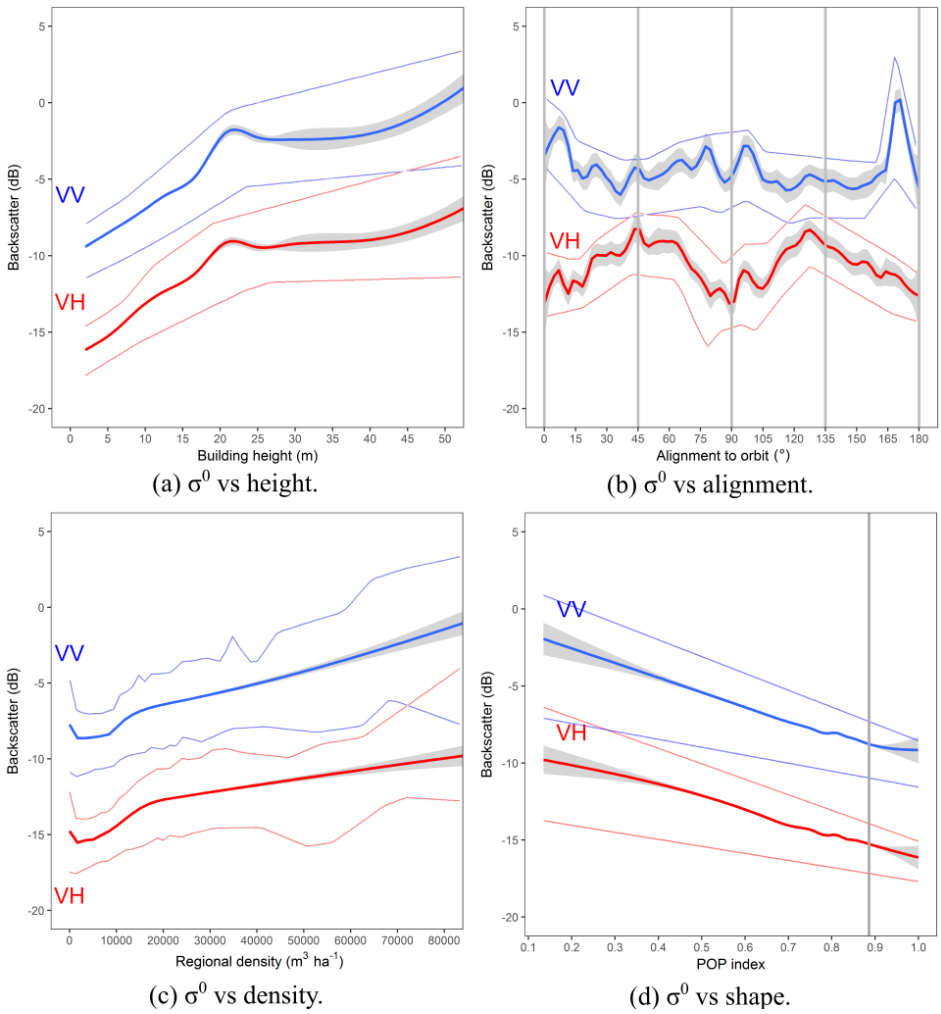

(a) σ^0 vs height. (b) σ^0 vs alignment.

(c) σ^0 vs density. (d) σ^0 vs shape.

Figure 3. VV and VH backscatter as a function of different physical parameters of buildings. Thick lines in (*a*)–(*d*) represent the mean backscatter values, grey area presents the confidence interval at the 0.95 level, and thin lines present the 0.25 and 0.75 quantiles. Source: Publication **II** Figures 6*(a)–(d)*.

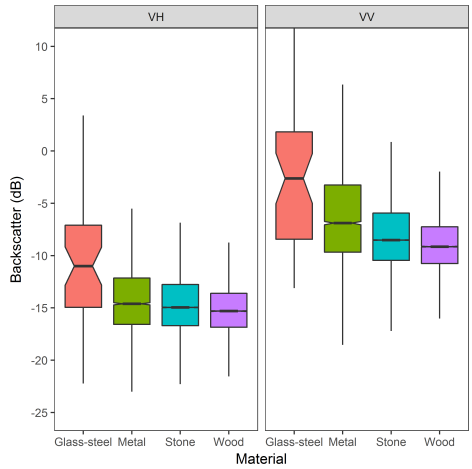

Figure 4. Backscatter σ^0 vs building's material. The box extends to first (Q1) and third (Q3) quartile values and the whiskers extend to 1.5 times interquartile range. The notches around median represent 95% confidence intervals. Source: Publication **II** Figure 6*(e)*.

are misattributed to pixels in front of the buildings This also explains why the peak aligns closely with the SAR ground-range resolution (20×22 m).

The alignment effect follows a 90° cycle (Figure 3(*b*)). VV backscatter peaks at 0°, 90° and 180°, and the VH peaks at 45° and 135° are consistent with the theoretical models (Lee and Pottier, 2009). This pattern indicates double-bounce scattering as the dominant mechanism. Further details are provided in section 3.2.2.

Backscatter increases by 5–6 dB with regional density (Figure3(*c*)). There is a peak at very low density: isolated buildings in low-density areas can produce stronger signals than clusters in tree-covered districts. Higher density generally correlates with taller and more voluminous buildings, enhancing backscatter. The direct relation of density to height, area, and volume complicates its role as an independent parameter.

Complex building shapes produce stronger backscatter (Figure 3(*d*)). Buildings with low POP values (close to 0) reflect up to 6 dB more than simpler shapes (POP near 1). Circular objects reflect less, while complex shapes with corners and niches increase dihedral and trihedral scattering.

The material of the building has also an impact on the backscatter (Figure 4). Glass and steel buildings show the strongest returns, followed by metal. Stone and wooden structures have similar backscatter. Also, material correlates with height. Tall buildings are often of glass or steel, while wood is a rare material for buildings above three floors. Although glass itself has low permittivity, its steel frames amplify backscatter. Detailed material analysis is limited due to constraints in the TAR database.

The correlation analysis aims to determine (a) which parameters affect backscatter strongly or weakly, (b) how building parameters influence the two

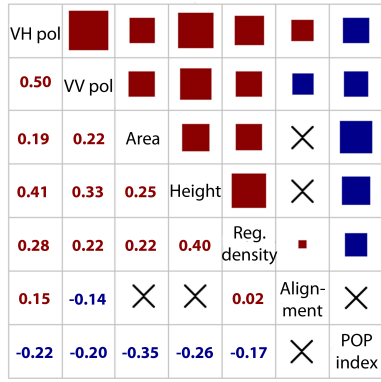

Figure 5. Correlogram of the physical parameters of buildings. Numbers indicate the correlation coefficients (Pearson's *r*). The size of the square indicates the relative strength of the correlation, and the cross shows that correlation is not statistically significant at the 0.001 level. Colour indicates the direction of the correlation (red for positive, blue for negative). Source: Publication **II** Figure 7.

polarisation channels, and (c) the extent of interdependence among parameters. A correlogram (Figure 5) visualises the strength and direction of the correlations between the pairs of variables.

The height of the building shows the strongest correlation with both polarisations, followed by the regional density, which is also strongly correlated with height ($r = 0.4$). The alignment to orbit has a weaker effect (Pearson's $r = 0.15$ for VH and -0.14 for VV) but varies: 0–45° alignment correlates positively with VH and negatively with VV. For analysis, alignment data (0–180°) were converted to 0–45°, assuming that one of the building facets always faces the SAR.

VH polarisation generally produces slightly higher correlation coefficients than the VV polarisation, making it more sensitive to parameter dynamics. This can aid in fine-tuning detection algorithms when combining channels.

The building parameters are highly interdependent. Taller buildings are typically in denser regions and have more complex shapes ($r = -0.26$). The alignment to orbit is independent of other parameters. The wall material was excluded due to its categorical nature.

3.2.2. Modelling of alignment effects

The backscattered power from an object depends on its geometrical properties, incidence angle, and look direction, and can vary more than 100 times (Lee and Pottier, 2009), potentially making some buildings invisible to urban detection methods. Thus, comprehensive modelling of alignment effects was performed in the study **II** to offer valuable insight for improving detection methods.

Role of geographic latitude. S1 in standard IW mode senses objects in Tallinn from two look directions and the corresponding incidence angles. The morning pass (descending orbit) looks from the SE-E, while the evening pass (ascending orbit) looks from the SW-W. The look direction varies with latitude, ranging from 98°/262° azimuth at the equator to 180°/0° near the poles.

It has been shown in Dong et al. (1997) and in Li et al. (2016) that especially in the case of shallow incidence angles (30–45°, like for S1 IW mode) the dominant scattering mechanism in the urban environment is dihedral scattering from wall-ground reflections. For co-polarised linear polarimetric channels such as VV or HH the dihedral scattering amplitude is maximum when the polarimetric orientation angle (POA) is either -90°, 0° or 90°, while it is minimum in the case of -45° or 45° POA. For cross-polarised polarimetric channels, such as VH or HV, it is the opposite. The dihedral scattering amplitude is minimum in the case of -90°, 0° or 90° POA, while it is maximum in the case of -45° or 45° POA. The building rotation angle ω ranges from -90° to 90°, with 0° in the case where the longer wall of the building is facing directly towards the radar look direction. POA and the rotation angle is related via the following equation (Iribe and Sato, 2007; Kimura et al., 2005; Li et al., 2016):

$$\mathrm{POA} = \frac{\tan(-\omega)}{\cos\theta} \tag{3.1}$$

where ω is the building rotation angle and θ is the incidence angle of S1.

A building has high backscatter and is well visible on a S1 SAR image in case a sufficiently large and high relative permittivity wall is facing straight towards the radar at 0° building rotation angle and 0° POA (co-pol. backscatter maximum at VV or HH). It can also be very well visible in the case of 45° POA (cross-pol. backscatter maximum at VH or HV) (Iribe and Sato, 2007), which corresponds to a 35° building rotation angle in the S1 IW far range and a 41° building rotation angle in S1 IW near range.

Role of building's rotation angle. To identify the SAR's "blind spots," backscatter relative power from two building types was modelled: (1) an oblong building with thin depth and wide width (Figure 6), and (2) a square-shaped building, using a dihedral model as in Lee and Pottier (2009). The rotation angle is related to the POA through equation 3.1, and the backscatter from a wall depends on the area facing the radar.

In Asian megacities (Figure 6(*a*) and (*b*)), backscatter from west-east orientated oblong buildings is very low, making them easily overlooked by detection algorithms. For near-range buildings with a rotation angle of 70–110° (relative to N), backscatter is about 3 times weaker (almost 5 dB) compared to when the longer wall faces the radar. In far range, this effect is even stronger. Buildings with rotation angles of 67–113° show 3 times weaker backscatter than the maximum. VV or VH backscatter from buildings with other rotation angles in either orbit should still provide a strong return on S1 radar images. In Tromsø, the gap between the peaks at 60° and 120° is narrower due to the shifted look directions (114° and 246° azimuth). The -5 dB point occurs at 85–95° for the near range and 81–99° for far range. Other rotation angles result in POAs near VV or VH maxima for both orbits, highlighting the benefits of using both S1 polarisations and orbits.

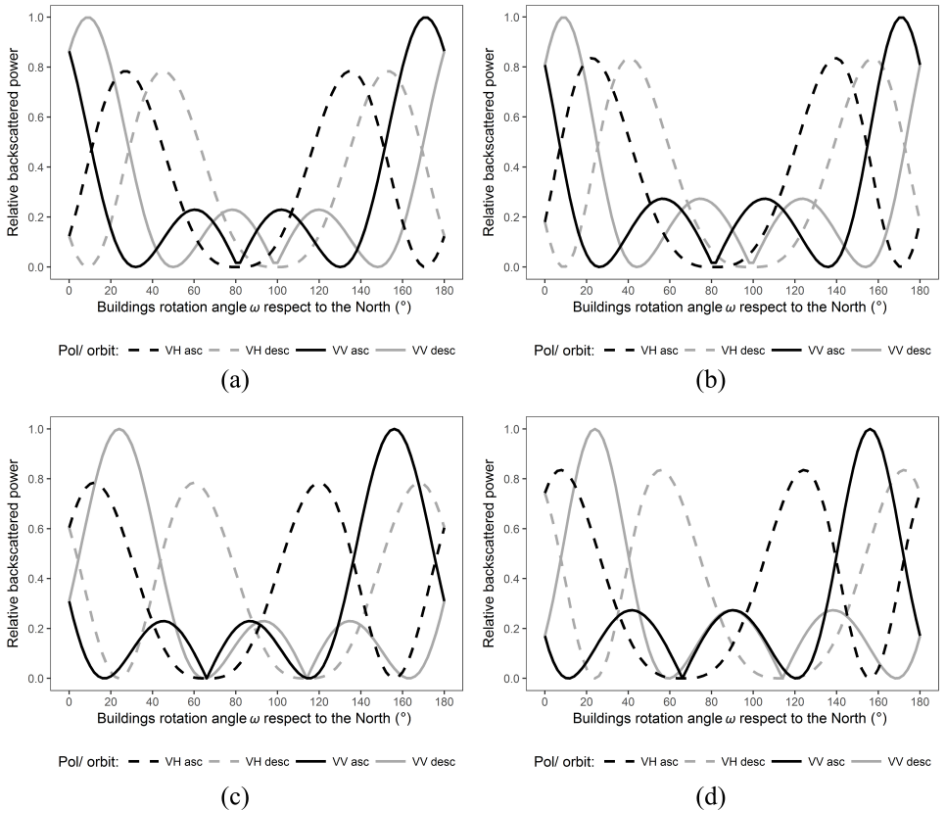

Figure 6. S1 backscatter for oblong buildings according to dihedral backscatter model in respect to building rotation angle (0° corresponds to the long wall being oriented in the north-south direction) for Asian megacities (25°N latitude) at near range (*a*) and far range (*b*), and for Tromso (69.7°N latitude) at near range (*c*) and far range (*d*). Source: Publication **II** Figure 11.

In the case of square-shaped buildings, no apparent "blind" regions (backscattered power < 0.4) due to low backscatter were observed (Figure in **II**, Figure 12). Backscatter from a building with a 45° rotation relative to the look direction is stronger in the VH channel than at the VV maximum when one wall is orthogonal to the radar, due to the larger projected wall area at this rotation. In Tromsø, the 132° difference between look directions causes the ascending VH and the descending VV maxima to overlap, as do the descending VH and ascending VV maxima. This creates narrow minima at 0°, 45°, 90°, and 135°, where the backscatter is about 2 times (3 dB) weaker than at the maxima.

3.3. Coherence time series for agricultural events detection

In the study **III** both aggregated S1 SAR coherence time series and time series of individual grassland parcels were analysed to make distinction between mowing and ploughing events.

3.3.1. Aggregated time series

The signatures γ_{vv} and γ_{vh} of mowing and ploughing events, along with the respective NDVI curves, are presented in Figure 7. For mowing, γ decreases gradually before the event, reaching a minimum just before the event, then rises to a maximum after the event, followed by a gradual decline. This behaviour is consistent with Section 2.4.4. The delay in maximum is due to the gradual drying of residual vegetation, which affects the SAR signal. The γ_{vv} and γ_{vh} signatures are closely aligned, indicating invariance to polarisation.

Mowing signatures are smoother because of more data points (1695 vs. 195 for ploughing). In contrast, ploughing exhibits greater variability, often linked to other management practices such as seeding or cultivation, which frequently occur near ploughing events.

Both mowing and ploughing show a minimum of coherence just before the

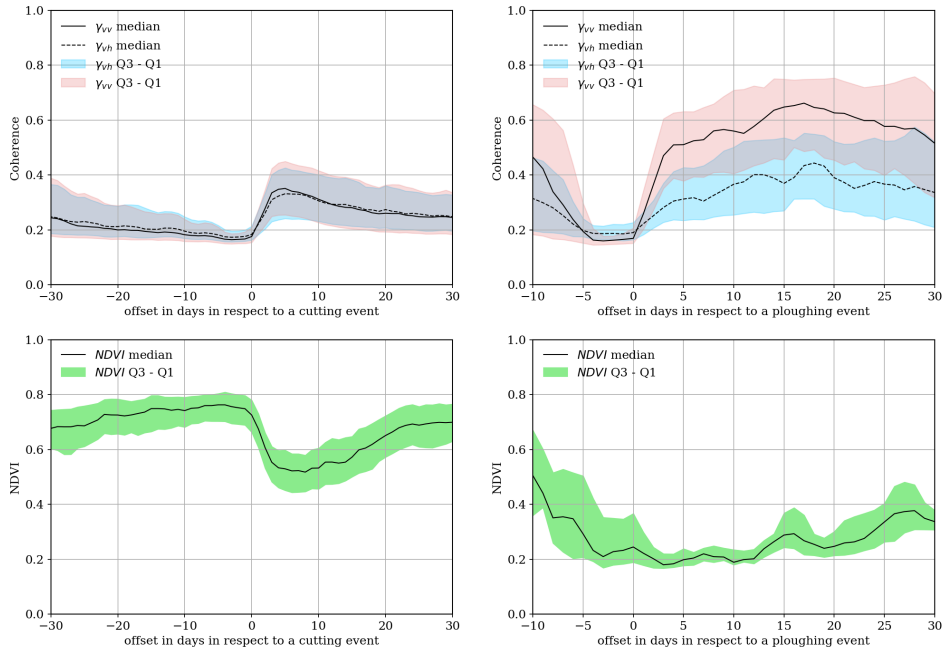

Figure 7. Median values of S1 coherence (top) and S2 NDVI (bottom) respect to mowing (left) and ploughing (right) events. Coloured regions represent the interquartile range. Events are from 2017, spanning between May and October (mowing), and June and September (ploughing). Source: Publication **III** Figure 3.

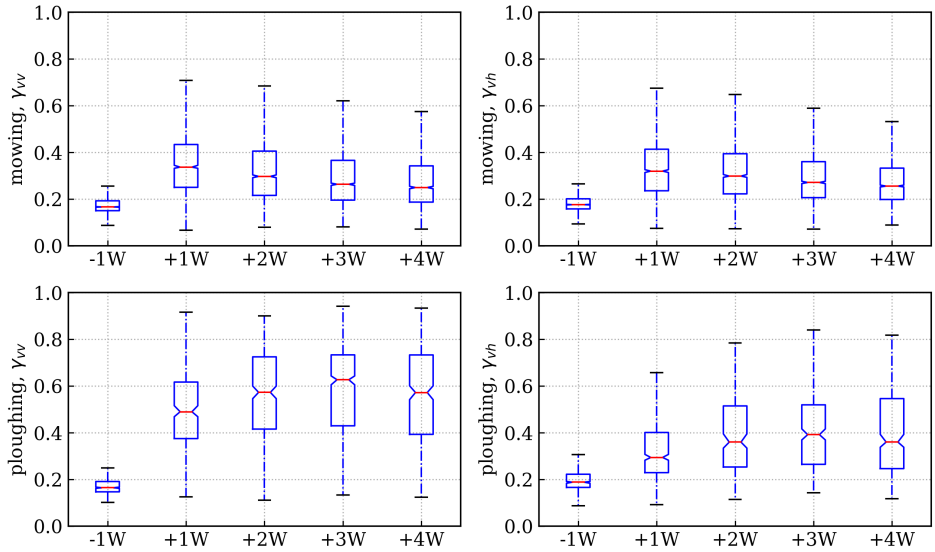

Figure 8. Evolution of γ over time around mowing and ploughing events represented by boxplots. Top row contains boxplots for mowing while the bottom one for ploughing. Left and right columns correspond to VV and VH polarization, respectively. Source: Publication **III** Figure 4.

event and a maximum after it. For ploughing, the maximum occurs later (10-20 days after the event), likely due to drying soil and decorrelation from moisture changes. Follow-up activities, such as fertilisation, also cause decorrelation, with coherence stabilising once activities cease. Unlike mowing, ploughing exhibits a polarisation dependence, with γ_{vv} significantly higher than γ_{vh} due to the soil structure favouring VV backscatter. This should be taken into account in management classification algorithms.

The NDVI signature for mowing inversely mirrors coherence, falling from 0.75 to 0.5 as γ increases from 0.18 to 0.35. For ploughing, NDVI remains stable at 0.2 for 12 days after the event, but shows greater variability afterward, influenced by grass types and follow-up activities. The pre-event NDVI for mowing is consistently high, reflecting tall, developed grasslands, while ploughing shows variable pre-event conditions, including bare fields, ploughed grass, or consecutive ploughing events.

To analyse γ dynamics around mowing and ploughing events, coherence values were divided into five time groups (Figure 8). The -1W group includes measurements where the first acquisition occurred 7 to 1 days before an event, while +1W corresponds to values from 1 to 7 days post-event, and so on. Measurements taken on the day of the event were excluded due to uncertainty in the activity timing. For mowing, the highest median γ_{vv} is observed in the +1W group (0.34), with an increase of 0.17 from -1W. Similarly, γ_{vh} increases by 0.14, from 0.18 at -1W to 0.32 at +1W. After the event, the difference between γ_{vv} and γ_{vh} remains small (around 0.02 units).

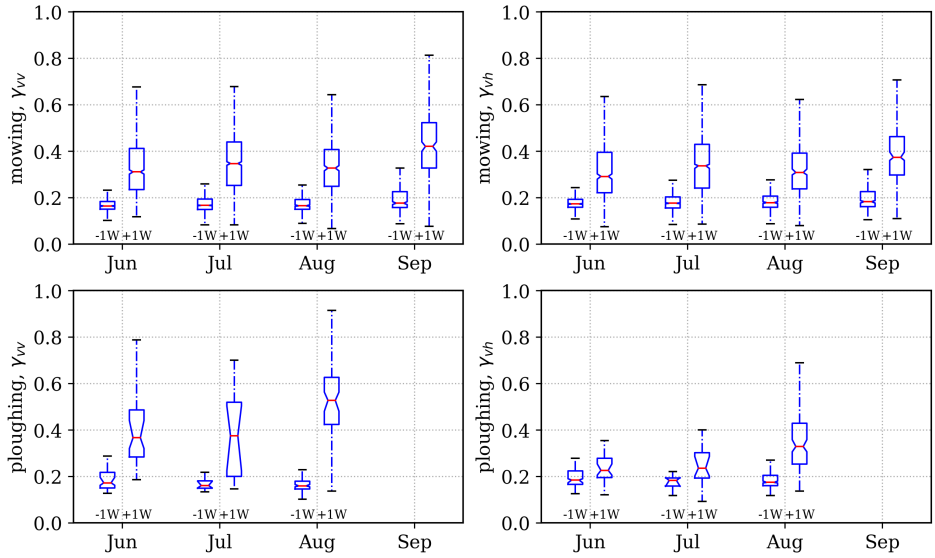

Figure 9. Boxplots of -1W and +1W subgroups defined by months when events were recorded. Top row contains boxplots for mowing while the bottom one for ploughing. Left and right columns correspond to VV and VH polarization, respectively. Source: Publication **III** Figure 5.

Ploughing shows larger polarisation differences. Between -1W and +1W, γ_{vv} increases by 0.33 and γ_{vh} by 0.10. The maximum values occur at +3W, reaching 0.63 for γ_{vv} and 0.39 for γ_{vh}.

Vegetation growth varies seasonally, which can influence results. To investigate, the -1W and +1W groups were further divided by month (Figure 9). For both types of events, the -1W values remain stable (0.16–0.18) throughout the season, while the +1W values show greater variability. For mowing, γ_{vv} medians increase from 0.31 in June to 0.35 in July, temporarily drop to 0.33 in August, and peak at 0.42 in September. γ_{vh} follows a similar pattern with slightly lower values. For ploughing, seasonal differences are more pronounced. +1W γ_{vv} increases by 0.16 between June and August, while γ_{vh} increases by 0.10 in the same period.

3.3.2. Time series of individual parcels

The general behaviour of S1 repeat-pass coherence is intuitive: short, sparse vegetation corresponds to high coherence, while tall, dense vegetation leads to low coherence. However, certain details must be considered for an accurate interpretation of coherence time series on individual parcels.

Time series from three different grassland parcels illustrate typical coherence dynamics in Northern Europe (Figure 10). The rain, marshland and ploughing effects shown were commonly observed in the 2017 dataset used in this study, providing information to improve monitoring systems for grasslands and other agricultural applications using S1 coherence time series.

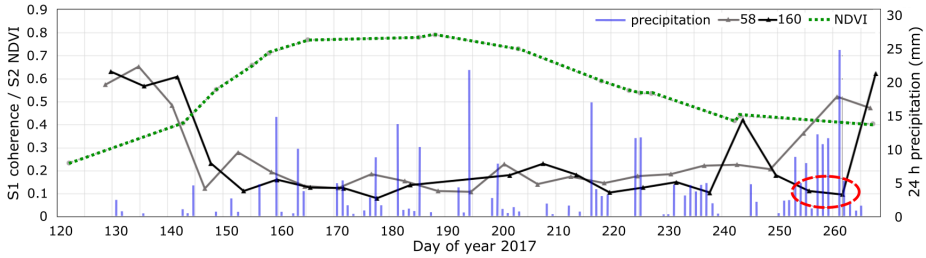

(a) effect of rain on coherence time series.

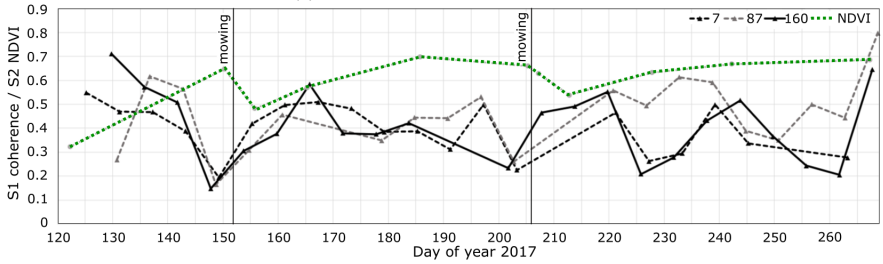

(b) coherence and NDVI time-series of a peatland-grassland parcel.

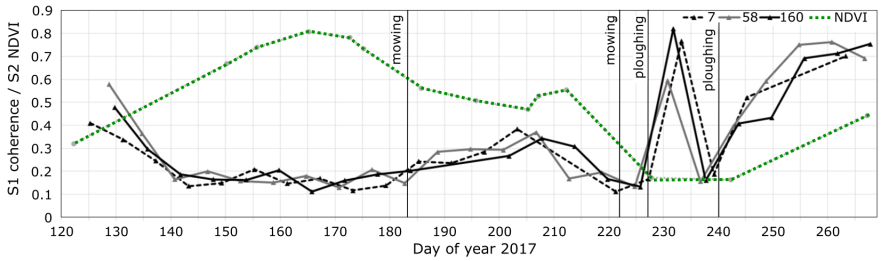

(c) coherence and NDVI time-series of a mowed and ploughed parcel.

Figure 10. S1 VV-coherence and NDVI time series of individual parcels: (a) unmown parcel affected by heavy rain (red circle notes the coherence data points affected by heavy rainfall), (b) grassland growing on a wet marshy soil, and (c) a parcel which was first mown and later ploughed. X-axis presents the day of year (DOY): "120" is April 30 and "260" is September 17. The lines in the gray-scale note the coherence time series from different orbits with relative orbit number (RON) brought in the legend. Green line notes the NDVI. Source: adopted from Publication **III** Figures 8–10.

In Figure 10*(a)*, an unmown grassland exhibits an inverse relationship between coherence and NDVI: NDVI follows a smooth arc, peaking mid-summer, while coherence is high in the early and late seasons but lower in the middle. Heavy rain significantly affects coherence. For example, on September 19 (DOY 262), an average precipitation of 22 mm was recorded during the preceding 6 hours at the Türi, Pajusi, and Viljandi weather stations. By this point, vegetation senescence is increasing coherence (RON 58 data points). However, rainfall caused a sharp drop in the coherence of RON 160 on DOYs 256 and 262, pushing it near the noise floor. Unlike farming events, which uniformly reduce coherence across all RONs, rainfall effects are localised, affecting only specific RONs due to altered

scattering properties at the time of S1 acquisition. As each image contributes to two interferometric pairs, the rainfall-induced coherence loss temporarily lowers two consecutive coherence values for a single RON. This distinction emphasises the utility of using multiple RONs in operational agricultural applications to differentiate rainfall effects from farming events.

Figure 10*(b)* illustrates S1 VV coherence and S2 NDVI for grasslands on peat soil. The coherence for unmown grass is higher (0.4–0.5) than for grass in mineral soils (below 0.2). NDVI is slightly lower, peaking at 0.7 compared to more than 0.8 for mineral soils. Coherence on peat soils is also more variable, fluctuating by 0.2 or more even without farming events, likely due to soil and vegetation moisture changes. The mowing signature on peat soils differs from that on mineral soils. In mineral soils, mowing transitions coherence from low to high. In peat soils, the coherence levels before and after mowing remain virtually unchanged, with only a temporary drop (0.15 to 0.25) just before mowing. However, it is important to note that all RONs are affected if the vegetation structure is completely changed by a mowing event that occurs between the acquisitions of an interferometric pair.

Figure10*(c)* shows coherence and NDVI of a mineral-soil grassland mown on DOYs 183 and 222, followed by ploughing on DOYs 227 and 240. After the first mowing, coherence increased from below 0.2 to 0.3, while NDVI decreased from 0.73 to 0.57. The second mowing had minimal effect due to ploughing five days later. However, the two ploughing events show distinct coherence signatures: coherence drops to near the noise floor just before ploughing and increases significantly afterward. Farming events affect all RONs uniformly, lowering the coherence for interferometric pairs where the event occurs. This behaviour contrasts with rainfall effects, which lower coherence for two consecutive pairs but only within specific RONs.

4. DISCUSSION

In this thesis, I investigated methods based on local area statistics from the S1 imagery for built-up area detection (**I**), then explored how different physical parameters of buildings influence the radar backscatter detected by S1 SAR (**II**), and finally analysed how mowing and ploughing activities in grasslands can be distinguished based on the analysis of SAR interferometric coherence and NDVI time series data (**III**). Firstly, I analysed how the built-up area methods performed under different settlement conditions and demonstrated that combining data from both orbits and polarisation channels yielded the highest accuracies (**I**). Secondly, I demonstrated, via quantitative statistical analysis, how the physical parameters of the buildings – such as height, alignment, material, density, and shape – impact the S1 backscatter, as well as modelled the alignment effects to detect potential "blind spots" (**II**). Finally, I demonstrated the distinct signatures of mowing and ploughing events, which can be detected with high confidence from the S1 coherence time series (**III**).

SAR is a highly promising remote sensing method for monitoring urban areas and agricultural grasslands across vast geographical regions. However, its accuracy and stability vary depending on geographical location, climate, and vegetation conditions. In this chapter, I discuss the limitations of SAR and provide additional context for interpreting the results.

4.1. Limitations for delineating urban areas

Urban detection methods based on local area backscatter statistics or image texture assume that building pixels are brighter than those of surrounding non-built-up areas. If this is not the case, buildings cannot be separated from the background. In the study **I** all built-up area detection methods demonstrated higher accuracy for the Tallinn study area, likely because built-up areas in Ida-Viru are more rural and therefore more vegetated. Similarly, within Tallinn, areas with greater vegetation coverage were classified with lower accuracy.

4.1.1. Problematic parameter ranges for building detection

To put the results of built-up area detections methods (**I**) and SAR sensitivity analysis (**II**) in the context I calculated the relative background level of S1 SAR backscatter. For that, I selected 25 non-built-up areas totalling 7.8 km^2 around Tallinn. These included forests, arable land, city parks and quarries, but no large water bodies. The mean backscatter values (σ^0 in dB) were calculated from the acquisition of the descending orbit on 28 March 2015, which was used as a reference for the image of the ascending orbit. The calculated background levels were -10.8 dB for VV and -16.7 dB for VH, while the mean backscatter from buildings was -7.95 dB for VV and -14.55 dB for VH.

Table 4. Problematic parameter ranges for the backscatter-based building detection. Problematic range is defined by a condition where the 0.25 quantile of the backscatter from buildings (Figure 3) is below the background level of the respective polarisation channel. The percentage shows how many observations within each defined parameter range are below the background level. The last column shows how many observations within each defined parameter range are below the background level in both channels at the same time. Source: adapted from Publication **II** Table 2.

	Problematic parameter range		Fraction (%) below background level from total observations		
Parameter	VH	VV	VH	VV	VH+VV
Height	<10 m	<5 m	24.1	10.8	5.71
Density	<15,000 m^3 ha^{-1}	<10,000 m^3 ha^{-1}	21.6	14.3	6.92
Shape	POP index > 0.6	POP index > 0.9	24.6	0.08	0.05
Material	wood, stone	wood, stone	12.1	10.5	2.40
Background level	<-16.7 dB	<-10.8 dB	25.4	21.7	9.79

An effective detection level was set at the 0.25 quantile of the building backscatter (Figure 3) and compared it to the calculated background levels. Background levels are sufficiently high to interfere with backscatter-based detection in problematic parameter ranges, as shown in Table 4.

For Tallinn, only 26 buildings (0.06%) meet these conditions for the VV channel, while 4419 buildings (10.8%) meet them for the VH channel. Despite a slightly stronger correlation between VH backscatter and building parameters (Figure 5), the VH channel is more affected by the higher background level than the VV channel. The backscatter from the buildings is clearer in the VV channel. However, combining both polarisations significantly improves the detection efficiency. Although 25.36% of the observations fall below the background level in the VH channel and 21.73% in the VV channel, only 9.79% fall below in both channels simultaneously. Using both polarisations and look directions can reduce these effects and prevent misclassification in methods relying on local backscatter statistics and texture.

4.1.2. The effect of the geographic latitude and alignment to orbit

Although the modelling of the buildings alignment in the study **II** was simplified, these models lead to several general conclusions. Detection of west-east oriented oblong buildings may be challenging at latitudes between 20° and 40°, and also further north with a narrower range of rotation angles. In the far range, the blind region in Asian megacities occurs for building rotation angles of 63–117° (Figure 6(*b*)), and in Tromsø for 80–100° (Figure 6(*d*)). At far range, dihedral backscatter from wall-ground reflections dominates over flat roof backscatter.

This can limit S1 data, which is otherwise well-suited for global built-up area mapping. Additional data sources, such as S2 optical data (Pesaresi et al., 2016), should be integrated into operational mapping systems. In Tallinn, the building backscatter distribution (Figure 3(*b*)) closely matches that of the extreme oblong buildings (Figure 6). The buildings are moderately oblong with a mean POP index of 0.78, corresponding to a 1:1.3 axis ratio (Figure 2(*d*)). This similarity could be amplified for two reasons: (a) the POP index simplifies the true 3D shape of buildings, underestimating more complex structures, and (b) taller buildings with complex shapes influence backscatter more than smaller cube-shaped houses, which are less visible.

4.2. Agricultural events reflected in coherence time series

The coherence time series of grassland parcels contains distinct patterns or signatures caused by farming events. Understanding these signatures is crucial for adapting satellite monitoring to CAP subsidy checks (Devos et al., 2018), where these signatures are also referred to as "markers."

The observed coherence behaviour in relation to the mowing and ploughing events (Figure 7) generally aligns with the theory outlined in Section 2.4.4. A notable detail is the delayed maximum coherence after mowing, likely due to residual vegetation taking time to dry and cease interaction with the SAR signal. Similar patterns are reported in S2 optical data, where the NDVI values remained relatively high immediately after mowing but decreased over time as the vegetation dried or was removed (Kolecka et al., 2018). The delay is even more pronounced for ploughing events, possibly due to soil drying and changes in moisture level between acquisitions, which initially cause decorrelation. Follow-up activities such as seeding and fertilisation further contribute to decorrelation, with coherence increases only after these activities cease.

Polarisation differences enable distinguishing mowing and ploughing. For both event types, coherence values typically reach a minimum just before the event due to profound changes in soil and vegetation caused by mowing or ploughing. γ_{vv} values are significantly higher than those of γ_{vh} after plowing, probably due to the overturned soil that favours the backscatter of VV. This distinction should be considered when designing algorithms to classify management practices.

The behaviour of NDVI around ploughing events is less clear. Variability after the event (12–30 days) can be influenced by differences in grass species and subsequent farming activities. NDVI values before events also vary widely, contrasting with mowing events, where high NDVI indicates well-developed grasslands.

Although the trends of γ_{vv} and γ_{vh} trends are broadly similar, the differences at the parcel level can be significant, reflecting differences in vegetation structure. For soil scattering, coherence is not dependent on polarisation whilst moisture is the primary factor (Zwieback et al., 2015). The absence of vegetation height data in this study limits interpretation, but previous research indicates typical heights

of unmown grass of 50 to 75 cm and heights of mown grass of 5 to 30 cm, with wet biomass ranging from 0.1 (mown) to 4.5 kg/m^2 (unmown) (Voormansik et al., 2013, 2015).

The coherence values before the event are stable, determined primarily by ENL in the coherence calculation (Lee and Pottier, 2009). Events between acquisitions cause total decorrelation, with a noise floor of 0.13 in this study. Missing S1 acquisitions for certain RONs had negligible effects on aggregated results, but could create gaps at the parcel level, potentially masking events in time series. Using multi-RON data helps mitigate the impact of missing acquisitions.

Rainfall introduces additional coherence loss, which affects individual RONs rather than all of them. Significant rainfall before SAR acquisition alters the scattering properties, lowering coherence in two consecutive pairs. Using multiple RONs helps to distinguish between rainfall and farming events, as traces of farming remain visible on unaffected RONs. The effects of rainfall are less pronounced during periods of high vegetation (DOY 150–230), where coherence is already low. For clearer analysis, short grass parcels near weather stations are recommended. Fluctuating coherence levels in peat-soil parcels are likely the result of changes in soil and vegetation moisture. High S1 coherence for peatland vegetation has been reported, linking coherence to the dynamics of the water regime (Tampuu et al., 2020).

4.3. Future work

This thesis concludes with recommended directions for future research:

- Exploring advanced SAR techniques, such as fully polarimetric SAR data, for enhanced urban mapping and agricultural monitoring.
- Applying machine learning and artificial intelligence to automate pattern recognition and time-series analysis.
- Validating the proposed methods in diverse geographic regions, including megacities and highly dynamic agricultural systems.

In this thesis, I established Sentinel-1 SAR data as a powerful resource for monitoring complex urban and agricultural systems, enabling the development of innovative applications for this purpose.

5. CONCLUSIONS

This thesis focuses on harnessing remote sensing data from the ESA Copernicus S1 SAR mission to address two primary applications: (1) monitoring urban areas to detect built-up structures and analyse how the main characteristics of the building impact backscatter values (**I**–**II**), and (2) identifying and classifying mowing and ploughing events on agricultural land to support EU CAP compliance monitoring and broader land use applications (**III**).

Three methods of local area statistics were applied to measure their precision in detecting built-up areas in the Tallinn and Ida-Viru study areas: mean-median (MM), speckle divergence (SD), and interferometric coherence (COH) (**I**). I proposed the MM method to provide a robust and computationally efficient method for large-scale urban monitoring. The difference between the local area mean and the local area median makes the assumption that the skewness of the distribution of the backscattering coefficient for different land use classes varies and is more skewed and asymmetric for urban targets compared to natural ones. The MM method achieved the highest accuracy for Tallinn (72%), while the SD method performed best for Ida-Viru (57%). Combining the data from both orbits and polarisation channels yielded the highest accuracies.

The physical parameters of the buildings, such as height, alignment, material, density, and shape, were quantitatively analysed to measure their impact on the S1 backscatter (**II**). Height has the strongest effect on backscatter values for both polarisation bands, with Pearson's r coefficients of 0.41 for VH and 0.33 for VV. The backscatter mean values increase steadily with increasing building height. The dihedral and trihedral structures that are common in urban areas return the backscatter to the same point on a radar image (Auer and Bamler, 2010), and the return is brighter, the greater the wall surface. It was also found that the close to linear dependence of backscatter on height saturates at 20 m due to the overlay effect at the 41–46° incidence angle S1 data in Tallinn, but for steeper incidence angles, the saturation is likely reached at even lower building heights, because of stronger overlay effects at steeper incidence angles. The alignment of the buildings to orbit has a relatively weaker effect (r = 0.15 for VH and -0.14 for VV) than other parameters. The effect of alignment is cyclical, with a cycle of 90° and our results were well in line with theoretical models (Lee and Pottier, 2009). It is interesting to note that the effect of alignment resembles more the modelled case for extreme oblong buildings than square-shaped plans, although the buildings in Tallinn are just moderately oblong (POP index mean value 0.78). The effect of the building density is moderate (r = 0.28 for VH and 0.22 for VV) and the same applies to building shape (r = 0.22 for VH and 0.20 for VV). Buildings made of glass, steel, or metal give strong backscatter, while backscatter mean values of wooden and stone buildings barely exceed 1–2 dB over background levels. Although the VH channel demonstrates a higher sensitivity to parameter variability than the VV channel in correlation analysis,

it is also more disturbed by the relatively high background backscattering level. The VV channel is more robust and less vulnerable to critical parameter ranges. Combining observations from both polarisation channels and both orbit directions substantially improves the detection efficiency. Future studies should analyse urban area detection methods in relation to results presented here with the aim of improving classification accuracy. In addition, a similar analysis as for Tallinn should be also performed for other cities with a different building stock, e.g. in America, Asia and Africa.

In case of agricultural grasslands, mowing and ploughing events can be detected from S1 coherence time series with high confidence (**III**). I demonstrated it based on a large ground reference data set that covers 1695 mowing and 195 ploughing events. Although vegetation is present, the values are close to the noise floor. For both event types, coherence tends to increase after an event as scattering from the soil becomes dominant. As the vegetation regrows, coherence slowly decreases to pre-event values. On average, ploughing causes a larger increase, at least for VV polarisation. In case of mowing, both polarizations exhibit very similar behavior to each other. Precipitation introduces variability into time series as moisture variations cause decorrelation that might mask out the increase due to events. In this respect, data density must be high if coherence is to be used for event detection. I discussed the effect of rainfall and farming events on S1 coherence time series and explained the means to distinguish them using the time series of alternative viewing geometries (different RONs). I also compared how the coherence time series for grassland in mineral soil differs from the one in peat soil. Although the results describe well the behavior of S1 coherence in agricultural grasslands of Northern European temperate climate, vegetation and management practices in the southern European Mediterranean climate can be remarkably different. Thus, further research in different climatic and agricultural conditions is needed, before S1 coherence time series could be used for operational grassland monitoring at Pan-European level and globally.

REFERENCES

Ainsworth, T. et al. (2008). Polarimetric SAR characterization of man-made structures in urban areas using normalized circular-pol correlation coefficients. *Remote Sens. Envir.*, 112(6):2876–2885.

Ali, I., Barrett, B., Cawkwell, F., Green, S., Dwyer, E., and Neumann, M. (2017). Application of repeat-pass TerraSAR-X staring spotlight interferometric coherence to monitor pasture biophysical parameters: Limitations and sensitivity analysis. *IEEE Journal of Selected Topics in Applied Earth Observations and Remote Sensing*, 10(7):3225–3231.

Askne, J., Santoro, M., Smith, G., and Fransson, J. E. S. (2003). Multitemporal repeat-pass SAR interferometry of boreal forests. *IEEE Transactions on Geoscience and Remote Sensing*, 41(7):1540–1550.

Auer, S. and Bamler, R. (2010). 3D analysis of trihedral reflection based on SAR simulation methods. In *Synthetic Aperture Radar (EUSAR), 2010 8th European Conference on*, pages 1–4. VDE.

Ban, Y. and Hu, H. (2007). RADARSAT fine-beam SAR data for land-cover mapping and change detection in the rural-urban fringe of the Greater Toronto Area. In *2007 Urban Remote Sensing Joint Event*, pages 1–7. IEEE.

Boots, B. and Okabe, A. (2007). Local statistical spatial analysis: Inventory and prospect. *International Journal of Geographical Information Science*, 21(3):355–375.

Brandon, P. S. (1977). *A Framework for Cost Exploration and Srtategic Cost Planning in Design*. Bristol University, Dept. of Architecture.

Bruzzone, L., Marconcini, M., Wegmuller, U., and Wiesmann, A. (2004). An advanced system for the automatic classification of multitemporal SAR images. *IEEE Transactions on Geoscience and Remote Sensing*, 42(6):1321–1334.

Chi, H., Sun, G., and Ling, F. (2009). Urban dynamic change detection using interferometric SAR in Southeast China. In *2009 Joint Urban Remote Sensing Event*, pages 1–9. IEEE.

Cloude, S. and Pottier, E. (1997). An entropy based classification scheme for land applications of polarimetric SAR. *IEEE Trans. Geosci. Remote Sens.*, 35(1):68–78.

Corbane, C., Faure, J.-F., Baghdadi, N., Villeneuve, N., and Petit, M. (2008). Rapid urban mapping using SAR/optical imagery synergy. *Sensors*, 8(11):7125–7143.

Cumming, I. G. and Wong, F. H. (2005). Digital processing of synthetic aperture radar data. *Artech house*, 1(2):3.

Dekker, R. (2003). Texture analysis and classification of ERS SAR images for map updating of urban areas in the Netherlands. *IEEE Trans. Geosci. Remote Sens.*, 41(9):1950–1958.

Del Frate, F., Pacifici, F., and Solimini, D. (2008). Monitoring urban land cover in Rome, Italy, and its changes by single-polarization multitemporal SAR images. *IEEE Journal of Selected Topics in Applied Earth Observations and Remote Sensing*, 1(2):87–97.

Dell'Acqua, F. and Gamba, P. (2003). Texture-based characterization of urban environments on satellite SAR images. *IEEE Trans. Geosci. Remote Sens.*, 41(1):153–159.

Dell'Acqua, F. and Gamba, P. (2006). Discriminating urban environments using multiscale texture and multiple SAR images. *International Journal of Remote Sensing*, 27(18):3797–3812.

Devos, W., Lemoine, G., Milenov, P., Fasbender, D., Loudjani, P., Wirnhardt, C., Sima, A., and Griffiths, P. (2018). Second discussion document on the introduction of monitoring to substitute OTSC: rules for processing applications in 2018-2019. JRC Science Hub.

Dong, Y., Forster, B., and Ticehurst, C. (1997). Radar backscatter analysis for urban environments. *International journal of remote sensing*, 18(6):1351–1364.

Erasmi, S. and Twele, A. (2009). Regional land cover mapping in the humid tropics using combined optical and SAR satellite data—a case study from Central Sulawesi, Indonesia. *International Journal of Remote Sensing*, 30(10):2465–2478.

ESA (2024a). Copernicus Sentinel-1: Earth Observation for Copernicus Programme. https://www.esa.int/Applications/Observing_the_Earth/Copernicus/Sentinel-1. [Accessed: 2024-11-19].

ESA (2024b). Sentinel-1 toolbox. https://step.esa.int/main/toolboxes/sentinel-1-toolbox/. [Accessed: 2024-11-27].

ESA (2024c). Speckle divergence operator documentation. https://step.esa.int/main/wp-content/help/versions/9.0.0/snap-toolboxes/org.esa.s1tbx.s1tbx.op.feature.extraction.ui/operators/SpeckleDivergence.html. [Accessed: 2024-11-23].

Esch, T. et al. (2010). Delineation of urban footprints from TerraSAR-X data by analyzing speckle characteristics and intensity information. *IEEE Trans. Geosci. Remote Sens.*, 48(2):905–916.

Esch, T. et al. (2013). Urban footprint processor–Fully automated processing chain generating settlement masks from global data of the TanDEM-X mission. *IEEE Geosci. Remote Sens. Lett.*, 10(6):1617–1621.

Estonian Land Board (2024). Estonian topographic database. https://geoportaal.maaamet.ee/eng/spatial-data/estonian-topographic-database-p305.html. [Accessed: 2024-11-27].

Estonian Weather Service (2024). Weather observations and data. https://www.ilmateenistus.ee/ilm/ilmavaatlused/vaatlusandmed/?lang=en. [Accessed: 2024-12-12].

Eurostat (2020). Share of main land types in utilised agricultural area (UAA) by NUTS 2 region. https://ec.europa.eu/eurostat/cache/metadata/en/tai05_esmsip2.htm. [Accessed: 2025-01-25].

Franceschetti, G., Iodice, A., and Riccio, D. (2002). A canonical problem in electromagnetic backscattering from buildings. *IEEE Transactions on Geoscience and Remote Sensing*, 40(8):1787–1801.

Gamba, P. et al. (2000). Detection and extraction of buildings from interferometric SAR data. *IEEE Trans. Geosci. Remote Sens.*, 38(1):611–617.

Garioud, A., Valero, S., Giordano, S., and Mallet, C. (2020). On the joint exploitation of optical and SAR imagery for grassland monitoring. In The International Archives of the Photogrammetry, Remote Sensing and Spatial Information Sciences.

Hagberg, J. O., Ulander, L. M. H., and Askne, J. (1995). Repeat-pass SAR interfer-

ometry over forested terrain. *IEEE Transactions on Geoscience and Remote Sensing*, 33(2):331–340.

Hanssen, R. F. (2001). *Radar interferometry: data interpretation and error analysis*, volume 2. Springer Science & Business Media.

Hastie, T. and Tibshirani, R. (1990). *Generalized Additive Models*. Chapman and Hall.

Henderson, F. M. (1982). An evaluation of Seasat SAR imagery for urban analysis. *Remote Sensing of Environment*, 12(6):439–461.

Hill, M. J. and et al. (2005). Integration of optical and radar classifications for mapping pasture type in Western Australia. *IEEE Transactions on Geoscience and Remote Sensing*, 43(7):1665–1681.

Hopkins, A. and Holz, B. (2006). Grassland for agriculture and nature conservation: production, quality and multi-functionality. *Agronomy research*, 4(1):3–20.

Houzelle, S. and Giraudon, G. (1991). Data fusion using SPOT and SAR images for bridge and urban area extraction. In *Geoscience and Remote Sensing Symposium, 1991. IGARSS'91. Remote Sensing: Global Monitoring for Earth Management., International*, volume 3, pages 1455–1458. IEEE.

Humboldt-Universität (2024). Accuracy assessment: User's accuracy and commission error. https://pages.cms.hu-berlin.de/EOL/geo_rs/S09_Accuracy_assessment.html#User%E2%80%99s_Accuracy__Commission_Error. [Accessed: 2024-11-27].

Iribe, K. and Sato, M. (2007). Analysis of polarization orientation angle shifts by artificial structures. *IEEE Transactions on Geoscience and remote sensing*, 45(11):3417–3425.

Just, D. and Bamler, R. (1994). Phase statistics of interferograms with applications to synthetic aperture radar. *Applied optics*, 33(20):4361–4368.

Khomarudin, R. and Indrajit, A. (2012). Combination of Speckle Divergence and Neighborhood Analysis to Classify Settlement from TerraSAR-X Data. *International Journal of Remote Sensing and Earth Sciences (IJReSES)*, 9.

Kimura, H., Papathanassiou, K. P., and Hajnsek, I. (2005). Polarization orientation effects in urban areas on SAR data. In *Proceedings. 2005 IEEE International Geoscience and Remote Sensing Symposium, 2005. IGARSS'05.*, volume 7, pages 4863–4867. IEEE.

Kolecka, N., Ginzler, C., Pazur, R., Price, B., and Verburg, P. H. (2018). Regional Scale Mapping of Grassland Mowing Frequency with Sentinel-2 Time Series. *Remote Sensing*, 10(8):1221.

Komisarenko, V., Voormansik, K., Elshawi, R., et al. (2022). Exploiting Time Series of Sentinel-1 and Sentinel-2 to Detect Grassland Mowing Events Using Deep Learning with Reject Region. *Scientific Reports*, 12(1):983.

Lavalle, M., Simard, M., and Hensley, S. (2012). A temporal decorrelation model for polarimetric radar interferometers. *IEEE Transactions on Geoscience and Remote Sensing*, 50(7):2880–2888.

Lee, J., Hoppel, K. W., Mango, S. A., and Miller, A. R. (1994). Intensity and phase statistics of multilook polarimetric and interferometric SAR imagery. *IEEE Transactions on Geoscience and Remote Sensing*, 32(5):1017–1028.

Lee, J.-S. and Pottier, E. (2009). *Polarimetric radar imaging: from basics to applications*. CRC Press.

Li, H., Li, Q., Wu, G., Chen, J., and Liang, S. (2016). The Impacts of Building Orientation on Polarimetric Orientation Angle Estimation and Model-Based Decomposition for

Multilook Polarimetric SAR Data in Urban Areas. *IEEE Transactions on Geoscience and Remote Sensing*, 54(9):5520–5532.

Liao, M., Jiang, L., Lin, H., Huang, B., and Gong, J. (2008). Urban change detection based on coherence and intensity characteristics of SAR imagery. *Photogrammetric Engineering & Remote Sensing*, 74(8):999–1006.

Lobert, F., Holtgrave, A.-K., Schwieder, M., Pause, M., Vogt, J., Gocht, A., and Erasmi, S. (2021). Mowing event detection in permanent grasslands: Systematic evaluation of input features from Sentinel-1, Sentinel-2, and Landsat 8 time series. *Remote Sensing of Environment*, 267:112751.

McNairn, H. and et al. (2009). Integration of optical and Synthetic Aperture Radar (SAR) imagery for delivering operational annual crop inventories. *ISPRS Journal of Photogrammetry and Remote Sensing*, 64(5):434–449.

Morishita, Y. and Hanssen, R. F. (2015). Temporal decorrelation in L-, C-, and X-band satellite radar interferometry for pasture on drained peat soils. *IEEE Transactions on Geoscience and Remote Sensing*, 53(2):1096–1104.

Moriyama, T. et al. (2005). Polarimetric SAR image analysis using model fit for urban structures. *IEICE Trans. Commun.*, 88(3):1234–1243.

Pesaresi, M., Corbane, C., Julea, A., Florczyk, A. J., Syrris, V., and Soille, P. (2016). Assessment of the added-value of Sentinel-2 for detecting built-up areas. *Remote Sensing*, 8(4):299.

Quartulli, M. and Datcu, M. (2004). Stochastic geometrical modeling for built-up area understanding from a single SAR intensity image with meter resolution. *IEEE Transactions on geoscience and remote sensing*, 42(9):1996–2003.

Reinermann, S., Gessner, U., Asam, S., Ullmann, T., Schucknecht, A., and Kuenzer, C. (2022). Detection of Grassland Mowing Events for Germany by Combining Sentinel-1 and Sentinel-2 Time Series. *Remote Sensing*, 14(7):1647.

Rocca, F. (2007). Modeling interferogram stacks. *IEEE Transactions on Geoscience and Remote Sensing*, 45(10):3289–3299.

Santoro, M., Wegmuller, U., and Askne, J. I. H. (2010). Signatures of ERS–Envisat interferometric SAR coherence and phase of short vegetation: An analysis in the case of maize fields. *IEEE Transactions on Geoscience and Remote Sensing*, 48(4):1702–1713.

Statistics Estonia (2024). Statistics Estonia Data Portal. https://andmed.stat.ee/en. [Accessed: 2024-11-24].

Strozzi, T. and Wegmuller, U. (1998). Delimitation of urban areas with SAR interferometry. In *Geosci. Remote Sens. Symposium Proc., IGARSS'98. 1998 IEEE Int.*, volume 3, pages 1632–1634. IEEE.

Tamm, T. (2018). *Use of Local Statistics in Remote Sensing of Grasslands and Forests*. PhD thesis, University of Tartu.

Tamm, T., Zalite, K., Voormansik, K., and Talgre, L. (2016). Relating Sentinel-1 interferometric coherence to mowing events on grasslands. *Remote Sensing*, 8(10):802.

Tampuu, T., Praks, J., Uiboupin, R., and Kull, A. (2020). Long Term Interferometric Temporal Coherence and DInSAR Phase in Northern Peatlands. *Remote Sensing*, 12(10):1566.

Taravat, A., Wagner, M., and Oppelt, N. (2019). Automatic Grassland Cutting Status Detection in the Context of Spatiotemporal Sentinel-1 Imagery Analysis and Artificial Neural Networks. *Remote Sensing*, 11(6):711.

Thiel, M., Esch, T., and Schenk, A. (2008). Object-oriented Detection of Urban Areas from TerraSAR-X Data. In *Proceedings of ISPRS 2008 Congress*, volume 37 of *Part B8, Commission VIII*, pages 23–27, Beijing.

Tison, C. et al. (2004). A new statistical model for Markovian classification of urban areas in high-resolution SAR images. *IEEE Trans. Geosci. Remote Sens.*, 42(10):2046–2057.

Touzi, R., Lopes, A., Bruniquel, J., and Vachon, P. W. (1999). Coherence estimation for SAR imagery. *IEEE Transactions on Geoscience and Remote Sensing*, 37(1):135–149.

UN-HABITAT (2024). World Cities Report 2024: Cities and Climate Action. https://unhabitat.org/sites/default/files/2024/11/wcr2024_-_full_report.pdf. [Accessed: 2024-12-31].

Vermeulen, S. et al. (2012). Options for support to agriculture and food security under climate change. *Environmental Science and Policy*, 15(1):136–144.

Voormansik, K. (2014). *X-band synthetic aperture radar applications for environmental monitoring*. PhD thesis, University of Tartu.

Voormansik, K., Jagdhuber, T., Olesk, A., Hajnsek, I., and Papathanassiou, K. P. (2013). Towards a Detection of Grassland Cutting Practices with Dual Polarimetric TerraSAR-X Data. *International Journal of Remote Sensing*, 34(22):8081–8103.

Voormansik, K., Jagdhuber, T., Zalite, K., Noorma, M., and Hajnsek, I. (2015). Observations of cutting practices in agricultural grasslands using polarimetric SAR. *IEEE Journal of Selected Topics in Applied Earth Observations and Remote Sensing*, 9(4):1382–1396.

Wegmuller, U. and Werner, C. (1997). Retrieval of vegetation parameters with SAR interferometry. *IEEE Transactions on Geoscience and Remote Sensing*, 35(1):18–24.

World Bank (2023). Urban development overview. https://www.worldbank.org/en/topic/urbandevelopment/overview. [Accessed: 2025-01-25].

Zalite, K. (2016). *Radar Remote Sensing for Monitoring Forest Floods and Agricultural Grasslands*. PhD thesis, University of Tartu.

Zalite, K., Antropov, O., Praks, J., Voormansik, K., and Noorma, M. (2016). Monitoring of agricultural grasslands with time series of X-band repeat-pass interferometric SAR. *IEEE Journal of Selected Topics in Applied Earth Observations and Remote Sensing*, 9(8):3687–3697.

Zebker, H. A. and Villasenor, J. (1992). Decorrelation in interferometric radar echoes. *IEEE Transactions on geoscience and remote sensing*, 30(5):950–959.

Zwieback, S., Hensley, S., and Hajnsek, I. (2015). Assessment of soil moisture effects on L-band radar interferometry. *Remote Sensing of Environment*, 164:77–89.

SUMMARY

This PhD thesis explores the use of Synthetic Aperture Radar (SAR) data from Sentinel-1 (S1), a mission of the European Space Agency (ESA), to advance urban and agricultural monitoring. With global urbanisation accelerating and agricultural land facing increasing demands, remote sensing provides a powerful means of accurate, scalable, and consistent monitoring. The research focuses on developing novel geoinformatic and SAR remote sensing methods to detect built-up areas, analyse urban structures, and identify key agricultural activities such as mowing and ploughing.

The main objectives of this thesis are: (a) investigating methods based on local area statistics from S1 imagery for built-up area detection (**I**); (b) exploring how different physical parameters of buildings influence the radar backscatter detected by S1 SAR (**II**); (c) distinguishing between mowing and ploughing activities in grasslands based on analysis of SAR interferometric coherence and NDVI time series data (**III**).

Three methods of local area statistics were applied to measure their precision in detecting built-up areas in the Tallinn and Ida-Viru study areas: mean-median (MM), speckle divergence (SD), and interferometric coherence (COH) (**I**). I proposed the MM method to provide a robust and computationally efficient method for large-scale urban monitoring. Experiments were conducted in two study areas in Estonia: Tallinn, the capital city, and Ida-Viru, a region with significant industrial activity and rural-urban dynamics. The results showed that the MM method achieved the highest accuracy in Tallinn (72%), while the SD method performed better in the more rural and vegetated Ida-Viru (57%). Combining dual polarisations (VV and VH) and data from ascending and descending orbits further improved accuracy. However, limitations were identified. Urban areas with dense vegetation, low-rise structures, or irregular building layouts were harder to detect. The findings underscore the importance of refining SAR-based urban detection methods by integrating additional data sources or exploring advanced techniques such as machine learning.

To improve urban monitoring, the thesis delves deeper into how building characteristics influence SAR backscatter (**II**). Factors such as height, alignment to orbit, shape, material, and regional density were analysed using data from Tallinn. Key findings include: (a) taller buildings produce stronger backscatter as a result of enhanced dihedral and trihedral scattering mechanisms; (b) the backscatter varies cyclically with the orientation of the building relative to the look direction of the radar; (c) glass and steel structures exhibited the highest backscatter, followed by metal, stone and wood; (d) regions with higher building density were correlated with stronger backscatter; (e) complex building shapes also amplified backscatter due to increased corner and edge reflections. The study highlights that the SAR sensitivity to building characteristics can both enhance and limit urban detection, e.g. specific building alignments or materials can create

radar 'blind spots', necessitating the integration of multiple viewing angles and polarizations to achieve satisfactory results.

In case of agricultural grasslands, mowing and ploughing events can be detected from S1 coherence time series with high confidence (**III**). Coherence measures the consistency of radar signals over time, which changes based on surface disturbances. A large-scale study analysed more than 1000 grassland parcels in Estonia, correlating the SAR coherence time series with reported agricultural activities. Key findings include: (a) grassland mowing events cause a sharp increase in SAR coherence values, as reduced vegetation height results in more consistent radar returns, providing a reliable and scalable method for detecting mowing activities; (b) ploughing events exhibited distinct temporal coherence trends compared to mowing, the coherence gradually increasing as the soil stabilises after disturbance; (c) Sentinel-1 SAR coherence time series proved effective in monitoring compliance with the EU Common Agricultural Policy (CAP). The methodology enables the cost-effective and large-scale detection of agricultural practices, reducing the reliance on labour-intensive field inspections.

This thesis concludes with recommended directions for future research:

- Exploring advanced SAR techniques, such as fully polarimetric SAR data, for enhanced urban mapping and agricultural monitoring.
- Applying machine learning and artificial intelligence to automate pattern recognition and time-series analysis.
- Validating the proposed methods in diverse geographic regions, including megacities and highly dynamic agricultural systems.

In this thesis, I established Sentinel-1 SAR data as a powerful resource for monitoring complex urban and agricultural systems, enabling the development of innovative applications for this purpose.

KOKKUVÕTE

Sentinel-1 tehisava-radari andmete kasutamine hoonestuse ja rohumaade kaugseires

Käesolev doktoritöö keskendub Euroopa Kosmoseagentuuri Copernicuse programmi Sentinel-1 missiooni (S1) tehisava-radari (SAR – *synthetic aperture radar*) andmete kasutamisele hoonestuse ja rohumaade kaugseires, viimase puhul konkreetsemalt põllumajanduslike tegevuste, nagu niitmine ja kündmine, tuvastamiseks.

SARil on optilise kaugseire ees olulisi eeliseid nagu sõltumatus pilvkattest ja päikesekiirgusest. Maapinnalt tagasihajuv radari signaal on tundlik pinnastruktuuri ja materjali füüsikaliste omaduste suhtes, mis muudab selle eriti kasulikuks tehisstruktuuride nagu hooned tuvastamisel, aga ka muutuste tuvastamiseks põllumajandusrakendustes, kuna saadaval on tihedad ja lünkadeta aegread.

Käesoleva töö peamisteks eesmärkideks on:

1. arendada arvutuslikult tõhusaid ja täpseid meetodeid hoonestatud alade tuvastamiseks, kasutades meetodina erinevaid SARil põhinevaid lokaalstatistikuid (publikatsioon **I**);
2. analüüsida, kuidas hoonete füüsikalised omadused (nt kõrgus, materjal ja orientatsioon) mõjutavad SARi signaali tagasihajumist (publikatsioon **II**);
3. tuvastada ja klassifitseerida niitmise ja kündmise sündmusi põllumajanduslikel rohumaadel, kasutades SARi interferomeetrilise koherentsuse aegridu (publikatsioon **III**).

Väitekirjas võrdlen kolme lokaalstatistikutel põhinevat hoonestuse tuvastamise meetodit (publikatsioon **I**): (a) lokaalse huviala pikslite signaali tagasihajumise intensiivsuse keskväärtuse ja mediaani vahe (MM – *mean minus median*), mis tugineb eeldusel, et tehisobjektidelt tagasikiirgava signaali väärtuste jaotus on asümmeetriline võrreldes loodusliku piirkonna signaali väärtuste normaaljaotusega; (b) haavelmüra lahknevus (SD – *speckle divergence*), mis tugineb SARi piltide tekstuuri varieeruvuse tuvastamisele eeldusel, et tehisobjektid tõstetakse esile nende suurema heterogeensuse tõttu; (c) interferomeetriline koherentsus (COH – *interferometric coherence*), mis võrdleb kahe eri ajal tehtud pildi sarnasust eeldusel, et tehislikud objektid on ajas stabiilsemad.

Hoonestuse muutuste suurema ja erisuunalise dünaamika tõttu valiti uurimisaladeks Tallinn selle valglinnastuva lähiümbruse ning kahaneva rahvastikuga Ida-Virumaa tööstuspiirkond. MM meetod saavutas kõrgeima täpsuse Tallinnas (72%), samas kui SD meetod oli sellest edukam Ida-Virumaal ja madalama ja hõredama hoonestusega maapiirkondades (57%). Sentinel-1 kahe polarimeetrilise kanali (VV, VH) ning kahe orbiidi (laskuv, tõusev) andmete kombineerimine parandas täpsust kõigi meetodite puhul. Siiski tuvastati ka piiranguid. Oodatult on tuvastus ebatäpsem madalama hoonestuse ja tihedama taimestikuga piirkondades, kus puuvõrad hooneid osaliselt varjavad. Need leiud rõhutavad vajadust

kaasata tuvastamise sisendina täiendavaid andmeallikaid ja suunavad kasutama võimsamaid nt masinõppel põhinevaid meetodeid.

Hoonete tuvastamisel on oluline, kuidas hoonete füüsilised parameetrid (kõrgus, orientatsioon orbiidi suhtes, hoone põhja kontuur, põhimaterjal ja hoonestuse piirkondlik tihedus) mõjutavad SARi signaali tagasihajumist (publikatsioon **II**). Andmestikuna kasutasin Tallinna ruumiandmete registrit. Peamised tulemused: (a) kõrgemad hooned tekitavad intensiivsemat tagasihajumist, kuna suurema peegeldava pinna tõttu on di- ja trihedraalsed peegeldusmehhanismid tugevamad. Siiski võivad väga kõrged hooned näidata nõrgemat tagasihajumist ülekattefektide (*overlay*) tõttu; (b) tagasihajumise intensiivsus varieerub tsükliliselt sõltuvalt hoone orientatsioonist radari vaatlussuunaga. VV kanal näitas tugevamaid tagasikiirguse väärtusi, kui hoonete seinad olid radari suhtes paralleelsed või risti, samas kui VH kanal saavutas intensiivsuse tipu diagonaalse orientatsiooni korral; (c) klaas- ja teraskonstruktsioonid näitasid intensiivsemat tagasihajumist, millele järgnesid metall ja kivi. Puithooned, mis on tavaliselt madalamad, näitasid nõrgemat signaali; (d) suurema hoonetihedusega piirkonnad olid seotud tugevama tagasihajumise tasemega. Keerulisemad hoonevormid näitasid suuremat tagasihajumist, mille põhjustab ilmselt reflektori efekt. SARi signaali tundlikkus hoonete erinevate parameetrite suhtes võib nii parandada kui ka piirata hoonete tuvastamise täpsust. Näiteks hoone teatud orientatsiooninurk võib muuta hooned SAR-ile nähtamatuks. Tulemuste parandamiseks tuleb kombineerida eri vaatenurki (orbiite) ja polarimeetrilisi kanaleid.

Väitekirjas demonstreerisin S1 andmete kasutatavust dünaamiliste nähtuste tuvastamiseks SARi interferomeetrilise koherentsuse aegridadest. Uuritavaks objektiks valitisin põllumajanduslike tööde nagu niitmise ja kündmise ajaliste markerite tuvastamine rohumaadel (publikatsioon **III**). Selle järgi on praktiline vajadus Euroopa Liidu ühise põllumajanduspoliitika nõuete täitmise järelvalve kontekstis. Koherentsus mõõdab SARi signaali ajalist stabiilsust – nt kõrge voogava heina korral on see vaikimisi madal, palja pinnase või madalama heina korral kõrgem, kukub see aga järsult kahe koherentsuse arvutamiseks kasutatud ülesvõtte vahel teostatud niitmise või kündmise töö korral. Analüüsi aluseks oli rohkem kui 1000 põllumajanduslikku rohumaad üle Eesti, mis on autorite andmeil kõige mahukam selletaoline uuring. Olulisemad tulemused on järgmised: (a) Niitmise sündmused rohumaadel põhjustavad SAR koherentsuse väärtuste järsu tõusu, kuna vähenenud taimestiku kõrgus tagab ühtlasema radari peegelduse. (b) Kündmise sündmused näitasid koherentsuse aegreas niitmisest eristuvat markerit, mille koherentsus suurenes pinnase stabiliseerudes nädalate jooksul järk-järgult. See võimaldab niitmise ja kündmise sündmuste täpset eristamist. Lõppjäreldusena on S1 SARi koherentsuse aegridade analüüs tõhus meetod ELi ühise põllumajanduspoliitika nõuete seireks. Metoodika võimaldab luua kulutõhusa ja laia geograafilise haardega põllumajandustööde seiresüsteemi ja vähendada kohapealsete inspektsioonide vajadust. KappaZeta OÜ arendas ja juurutas S1 andmetel põhineva rohumaade niitmise tuvastamise süsteemi Põllumajanduse Registrite ja Informatsiooni Ameti tellimusel 2019. aasta alguses.

Lõpetan väitekirja üldiste soovitustega edasisteks uuringuteks:

- SARi põhiste meetodite täiendamine, sh täispolarimeetrilise SARi andmete uurimine hoonestuse- ja põllumajanduse seires.
- Täiendavate andmeallikate kombineerimine, sh SARi ja optilise kaugseire andmestike ühendamine, et ületada mõlema fundamentaalsed piirangud.
- Tehisintellekti ja masinõppe laialdasem rakendamine sekundaarsete sisendtunnuste genereerimiseks, aegridade analüüsiks ja mustrite tuvastamiseks.
- Meetodite rakendamine ja valideerimine erinevates geograafilistes ja klimaatilistes piirkondades üle maailma.

Käesolevas väitekirjas demonstreerisin S1 SAR andmete kasutamise suurt potentsiaali linnaliste ja põllumajanduslike süsteemide seires ja andsin positiivse väljavaate uuenduslike rakenduste loomiseks.

ACKNOWLEDGEMENTS

I am deeply grateful to my former colleagues and co-authors at KappaZeta Ltd.: Kaupo Voormansik, Karlis Zalite, and Tanel Tamm. Special thanks to Kaupo, my co-author, who initiated the SAR research group and invited me to join. Kaupo's guidance shaped all the research behind this work.

I cordially thank Karlis Zalite, my closest co-author, for his collaboration, contribution, constructive feedback, and encouragement in the final phase of writing this thesis.

I also appreciate all my other co-authors: Anni Seiler (Sisas), Jaan Praks, Mart Noorma, Thomas Jagdhuber, Indrek Sünter, Tarvi Verro, Agris Brauns, and Dainis Jakovels. Your contributions were invaluable.

My sincere gratitude goes to my supervisor, Prof. Tõnu Oja, for his wise advice, patience, and fatherly support throughout this process.

I heartily thank Aire Olesk and Kadri Koorem for their reviews and suggestions to polish the final version of this thesis. Aire, you are a true friend in the end.

I am grateful to my STACC colleagues, Jane Luht, Evely Kukk, and Tiit Sepp, for motivating me and stepping in to cover my responsibilities during the intensive periods of writing this thesis. Your understanding and support have meant a lot to me.

My heartfelt thanks also go to Tõravere Observatory and its former director, Anu Noorma, for fostering a supportive research environment, which played a vital role in bootstrapping KappaZeta Ltd. as well as in shaping this thesis.

Thanks to the Estonian Land Board for the nDSM database, the Tallinn City Administration for the Spatial Data Register (TAR), the Estonian Agricultural Registers, and the farmers who contributed essential data.

This work was supported by the projects "Data Analytics for Optimising Agricultural Monitoring," funded by STACC OÜ through Enterprise Estonia's Competence Centre programme (projects No. EU30015 and EU48684), and STACC's regular base funding for R&D from the Ministry of Education and Research.

Finally, my deepest thanks to my family, especially to my life partner, Merle Kusma, for her unwavering support, patience, and indulgent understanding.

PUBLICATIONS

CURRICULUM VITAE

Personal data

Name:	Kalev Koppel
Date, place of birth:	15.06.1979, Hiiumaa county
Nationality:	Estonian
Current employment:	STACC OÜ, CEO
Address:	STACC OÜ, Narva mnt 20, 51009 Tartu, Estonia
E-mail:	kalev.koppel@stacc.ee
Phone:	+372 515 9966

Education

2011–...	University of Tartu, Faculty of Science and Technology, Institute of Ecology and Earth Sciences, Department of Geography, *PhD* studies in Geoinformatics
2004–2005	Lund University, Centre for Geographical Information Systems, guest researcher
2002–2005	University of Tartu, Faculty of Philosophy, Institute of History and Archaeology, master's degree (*MA*) in Archival Studies
2001–2002	Uppsala University, Master's program in Cultural and Economic Geography
1997–2002	University of Tartu, Faculty of Philosophy, Institute of History and Archaeology, bachelor degree (*BA*) in Archival Studies
1994–1997	Noarootsi Gymnasium

Employment

2024–...	Metrosert Ltd., member of the advisory board on health data
2023–...	Grab2Go Ltd., member of the supervisory board
2019–...	STACC Ltd., CEO, member of the board
2016–2019	KappaZeta Ltd., CEO, co-founder
2016–2018	Tartu Observatory, researcher, project manager
2013–2016	STACC Ltd., CEO, member of the board
2009–2012	Regio Ltd., business unit manager, GIS software development
2006–2009	Regio Ltd., IT project manager
2005–2006	Regio Ltd., cartographer
2002–2005	Estonian Historical Archives, cartography expert - archivist

Scientific work

Main fields of interest:

Natural Sciences and Engineering – Radar remote sensing
Natural Sciences and Engineering – Artificial intelligence

Academic degree

Kalev Koppel, Research Master's Degree, 2005, (sup) Aadu Must; Siim Veski. The research methods of historical land use as exemplified by the formation of rural landscapes in the Kasaritsa study area (Rõuge parish) in the 17th–19th centuries. University of Tartu, Faculty of Philosophy, Institute of History and Archaeology, Chair of Archival Studies.

Publications

1. Konsa, Kurmo; Treimann, Meri Liis; Piirisild, Kristiina; Koppel, Kalev (2023). Machine learning model for the prediction of condition of museum objects. International Journal of Conservation Science, 14 (4), 1343–1350.
2. Voormansik, Kaupo; Zalite, Karlis; Sunter, Indrek; Tamm, Tanel; Koppel, Kalev; Verro, Tarvi; Brauns, Agris; Jakovels, Dainis; Praks, Jaan (2020). Separability of Mowing and Ploughing Events on Short Temporal Baseline Sentinel-1 Coherence Time Series. Remote Sensing, 12 (22), ARTN 3784.
3. Koppel, Kalev; Zalite, Karlis; Voormansik, Kaupo; Jagdhuber, Thomas; (2017). Sensitivity of Sentinel-1 backscatter to characteristics of buildings. International Journal of Remote Sensing, 38 (22), 6298–6318.
4. Koppel, Kalev; Zalite, Karlis; Sisas, Anni; Voormansik, Kaupo; Praks, Jaan; Noorma, Mart (2015). Sentinel-1 for urban area monitoring — Analysing local-area statistics and interferometric coherence methods for buildings' detection. Geoscience and Remote Sensing Symposium (IGARSS), 2015 IEEE International: 2015 IEEE International Geoscience and Remote Sensing Symposium (IGARSS). IEEE, 1175–1178.
5. Reisberg, S ; Talvik, H-A; Koppel, K; Laur, S; Vilo, J (2015). Description of the current status and future needs of the Information Architecture and Data Management solutions for the national personalised medicine pilot project. 1–100.
6. Poska, A.; Saarse, L.; Koppel., K.; Nielsen, A.B.; Avel, E.; Vassiljev, J.; Väli, V. (2014). The Verijärv area, South Estonia over the last millennium: A high resolution quantitative landcover reconstruction based on pollen and historical data. Review of Palaeobotany and Palynology, 207, 5–17.
7. Poska, Anneli; Sepp, Edgar; Veski, Siim; Koppel, Kalev (2008). Using quantitative pollen-based land-cover estimations and a spatial CA_Markov model to reconstruct the development of cultural landscape at Rõuge, South Estonia. Vegetation History and Archaeobotany, 17 (5), 527–541.

8. Veski, S.; Koppel, K.; Poska, A. (2005). Integrated palaeoecological and historical data in the service of fine-resolution land use and ecological change assessment during the last 1000 years in Rouge, southern Estonia. Journal of Biogeography, 32 (8), 1473–1488.
9. Veski, Siim; Heinsalu, Atko; Koppel, Kalev (2003). Lehitsedes esimesi lehekülgi Rõuge järvemuda raamatust. Eesti Loodus, 1, 6–11.
10. Koppel, K. (2002). Kuidas kaardid kõnelesid: 17.-19. sajandi katastriplaanide esitusmudel. Ajalooline Ajakiri The Estonian Historical Journal, 9(16), 13–32.
11. Koppel, K. (2002). GIS on tööriist: geograafilise infosüsteemi rakendamisest ajalooliste katastrimaterjalide uurimisel. Ajalooline Ajakiri The Estonian Historical Journal, 2001/4, 87–104.

ELULOOKIRJELDUS

Isikuandmed

Nimi:	Kalev Koppel
Sünniaeg ja -koht:	15.06.1979, Hiiumaa, Emmaste vald
Kodakondsus:	Eesti
Praegune töökoht:	STACC OÜ, tegevjuht
Aadress:	STACC OÜ, Narva mnt 20, 51009 Tartu, Eesti
E-post:	kalev.koppel@stacc.ee
Telefon:	+372 515 9966

Haridus

2011–...	Tartu Ülikooli loodus- ja täppisteaduste valdkond, ökoloogia ja maateaduste instituut, geoinformaatika eriala doktoriõpe
2004–2005	Lundi Ülikool, geoinformaatika keskus (Centre for Geographical Information Systems), külalisüliõpilane Rootsi instituudi stipendiumiga
2002–2005	Tartu Ülikool, ajaloo osakond, arhiivinduse eriala magistriõpe
2001–2002	Uppsala Ülikool, inim- ja majandusgeograafia magistriprogramm
1997–2002	Tartu Ülikool, ajaloo osakond, arhiivinduse ja arheoloogia eriala bakalaureuseõpe
1994–1997	Noarootsi Gümnaasium

Teenistuskäik

2024–...	Metrosert AS, terviseandmete valdkonna nõukoja liige
2023–...	Grab2Go AS, nõukogu liige
2019–...	Andmeteadusettevõte STACC OÜ, tegevjuht, juhatuse liige
2016–2019	KappaZeta OÜ, tegevjuht, kaasasutaja
2016–2018	Tartu Observatoorium, teadur, projektijuht
2013–2016	STACC OÜ, tegevjuht, juhatuse liige
2009–2012	Regio AS, GIS tarkvara äriüksuse juht
2006–2009	Regio AS, projektijuht
2005–2006	Regio AS, kartograaf
2002–2005	Eesti Ajalooarhiiv, arhivaar, ajaloolise kartograafia ekspert

Teadustegevus

Peamised uurimisvaldkonnad

Loodusteaduse ja tehnika – radarkaugseire
Loodusteaduse ja tehnika – tehisintellekt

Akadeemiline kraad

Kalev Koppel, magistrikraad (teaduskraad), 2005, (juh) Aadu Must; Siim Veski, Maakasutuse uurimise metoodika Kasaritsa uurimisala (Rõuge kihelkond) 17.-19. sajandi külamaastike kujunemise näitel, Tartu Ülikool, Filosoofiateaduskond, Ajaloo ja arheoloogia instituut, Arhiivinduse õppetool.

Publikatsioonid

1. Konsa, Kurmo; Treimann, Meri Liis; Piirisild, Kristiina; Koppel, Kalev (2023). Machine learning model for the prediction of condition of museum objects. International Journal of Conservation Science, 14 (4), 1343–1350.
2. Voormansik, Kaupo; Zalite, Karlis; Sunter, Indrek; Tamm, Tanel; Koppel, Kalev; Verro, Tarvi; Brauns, Agris; Jakovels, Dainis; Praks, Jaan (2020). Separability of Mowing and Ploughing Events on Short Temporal Baseline Sentinel-1 Coherence Time Series. Remote Sensing, 12 (22), ARTN 3784.
3. Koppel, Kalev; Zalite, Karlis; Voormansik, Kaupo; Jagdhuber, Thomas; (2017). Sensitivity of Sentinel-1 backscatter to characteristics of buildings. International Journal of Remote Sensing, 38 (22), 6298–6318.
4. Koppel, Kalev; Zalite, Karlis; Sisas, Anni; Voormansik, Kaupo; Praks, Jaan; Noorma, Mart (2015). Sentinel-1 for urban area monitoring — Analysing local-area statistics and interferometric coherence methods for buildings' detection. Geoscience and Remote Sensing Symposium (IGARSS), 2015 IEEE International: 2015 IEEE International Geoscience and Remote Sensing Symposium (IGARSS). IEEE, 1175–1178.
5. Reisberg, S ; Talvik, H-A; Koppel, K; Laur, S; Vilo, J (2015). Description of the current status and future needs of the Information Architecture and Data Management solutions for the national personalised medicine pilot project. 1–100.
6. Poska, A.; Saarse, L.; Koppel., K.; Nielsen, A.B.; Avel, E.; Vassiljev, J.; Väli, V. (2014). The Verijärv area, South Estonia over the last millennium: A high resolution quantitative landcover reconstruction based on pollen and historical data. Review of Palaeobotany and Palynology, 207, 5–17.
7. Poska, Anneli; Sepp, Edgar; Veski, Siim; Koppel, Kalev (2008). Using quantitative pollen-based land-cover estimations and a spatial CA_Markov model to reconstruct the development of cultural landscape at Rõuge, South Estonia. Vegetation History and Archaeobotany, 17 (5), 527–541.

8. Veski, S.; Koppel, K.; Poska, A. (2005). Integrated palaeoecological and historical data in the service of fine-resolution land use and ecological change assessment during the last 1000 years in Rouge, southern Estonia. Journal of Biogeography, 32 (8), 1473–1488.
9. Veski, Siim; Heinsalu, Atko; Koppel, Kalev (2003). Lehitsedes esimesi lehekülgi Rõuge järvemuda raamatust. Eesti Loodus, 1, 6–11.
10. Koppel, K. (2002). Kuidas kaardid kõnelesid: 17.-19. sajandi katastriplaanide esitusmudel. Ajalooline Ajakiri The Estonian Historical Journal, 9(16), 13–32.
11. Koppel, K. (2002). GIS on tööriist: geograafilise infosüsteemi rakendamisest ajalooliste katastrimaterjalide uurimisel. Ajalooline Ajakiri The Estonian Historical Journal, 2001/4, 87–104.

DISSERTATIONES GEOGRAPHICAE UNIVERSITATIS TARTUENSIS

1. **Вийви Руссак.** Солнечная радиация в Тыравере. Тарту, 1991.
2. **Urmas Peterson.** Studies on Reflectance Factor Dynamics of Forest Communities in Estonia. Tartu, 1993.
3. **Ülo Suursaar.** Soome lahe avaosa ja Eesti rannikumere vee kvaliteedi analüüs. Tartu, 1993.
4. **Kiira Aaviksoo.** Application of Markov Models in Investigation of Vegetation and Land Use Dynamics in Estonian Mire Landscapes. Tartu, 1993.
5. **Kjell Weppling.** On the assessment of feasible liming strategies for acid sulphate waters in Finland. Tartu, 1997.
6. **Hannes Palang.** Landscape changes in Estonia: the past and the future. Tartu, 1998.
7. **Eiki Berg.** Estonia's northeastern periphery in politics: socio-economic and ethnic dimensions. Tartu, 1999.
8. **Valdo Kuusemets.** Nitrogen and phosphorus transformation in riparian buffer zones of agricultural landscapes in Estonia. Tartu, 1999.
9. **Kalev Sepp.** The methodology and applications of agricultural landscape monitoring in Estonia. Tartu, 1999.
10. **Rein Ahas.** Spatial and temporal variability of phenological phases in Estonia. Tartu, 1999.
11. **Эркки Таммиксаар.** Географические аспекты творчества Карла Бэра в 1830–1840 гг. Тарту, 2000.
12. **Garri Raagmaa.** Regional identity and public leaders in regional economic development. Tartu, 2000.
13. **Tiit Tammaru.** Linnastumine ja linnade kasv Eestis nõukogude aastatel. Tartu, 2001.
14. **Tõnu Mauring.** Wastewater treatment weltlands in Estonia: efficiency and landscape analysis. Tartu, 2001.
15. **Ain Kull.** Impact of weather and climatic fluctuations on nutrient flows in rural catchments. Tartu, 2001.
16. **Robert Szava-Kovats.** Assessment of stream sediment contamination by median sum of weighted residuals regression. Tartu, 2001.
17. **Heno Sarv.** Indigenous Europeans east of Moscow. Population and Migration Patterns of the Largest Finno-Ugrian Peoples in Russia from the 18th to the 20th Centuries. Tartu, 2002.
18. **Mart Külvik.** Ecological networks in Estonia — concepts and applications. Tartu, 2002.
19. **Arvo Järvet.** Influence of hydrological factors and human impact on the ecological state of shallow Lake Võrtsjärv in Estonia. Tartu, 2004.
20. **Katrin Pajuste.** Deposition and transformation of air pollutants in coniferous forests. Tartu, 2004.

21. **Helen Sooväli.** *Saaremaa waltz*. Landscape imagery of Saaremaa Island in the 20th century. Tartu, 2004.
22. **Antti Roose.** Optimisation of environmental monitoring network by integrated modelling strategy with geographic information system — an Estonian case. Tartu, 2005.
23. **Anto Aasa.** Changes in phenological time series in Estonia and Central and Eastern Europe 1951–1998. Relationships with air temperature and atmospheric circulation. Tartu, 2005.
24. **Anneli Palo.** Relationships between landscape factors and vegetation site types: case study from Saare county, Estonia. Tartu, 2005.
25. **Mait Sepp.** Influence of atmospheric circulation on environmental variables in Estonia. Tartu, 2005.
26. **Helen Alumäe.** Landscape preferences of local people: considerations for landscape planning in rural areas of Estonia. Tartu, 2006.
27. **Aarne Luud.** Evaluation of moose habitats and forest reclamation in Estonian oil shale mining areas. Tartu, 2006.
28. **Taavi Pae.** Formation of cultural traits in Estonia resulting from historical administrative division. Tartu, 2006.
29. **Anneli Kährik.** Socio-spatial residential segregation in post-socialist cities: the case of Tallinn, Estonia. Tartu, 2006.
30. **Dago Antov.** Road user perception towards road safety in Estonia. Tartu, 2006.
31. **Üllas Ehrlich.** Ecological economics as a tool for resource based nature conservation management in Estonia. Tartu, 2007.
32. **Evelyn Uuemaa.** Indicatory value of landscape metrics for river water quality and landscape pattern. Tartu, 2007.
33. **Raivo Aunap.** The applicability of gis data in detecting and representing changes in landscape: three case studies in Estonia. Tartu, 2007.
34. **Kai Treier.** Trends of air pollutants in precipitation at Estonian monitoring stations. Tartu, 2008.
35. **Kadri Leetmaa.** Residential suburbanisation in the Tallinn metropolitan area. Tartu, 2008.
36. **Mare Remm.** Geographic aspects of enterobiasis in Estonia. Tartu, 2009.
37. **Alar Teemusk.** Temperature and water regime, and runoff water quality of planted roofs. Tartu, 2009.
38. **Kai Kimmel.** Ecosystem services of Estonian wetlands. Tartu, 2009.
39. **Merje Lesta.** Evaluation of regulation functions of rural landscapes for the optimal siting of treatment wetlands and mitigation of greenhouse gas emissions. Tartu, 2009.
40. **Siiri Silm.** The seasonality of social phenomena in Estonia: the location of the population, alcohol consumption and births. Tartu, 2009.
41. **Ene Indermitte.** Exposure to fluorides in drinking water and dental fluorosis risk among the population of Estonia. Tartu, 2010.
42. **Kaido Soosaar.** Greenhouse gas fluxes in rural landscapes of Estonia. Tartu, 2010.

43. **Jaan Pärn.** Landscape factors in material transport from rural catchments in Estonia. Tartu, 2010.
44. **Triin Saue.** Simulated potato crop yield as an indicator of climate variability in Estonia. Tartu, 2011.
45. **Katrin Rosenvald.** Factors affecting EcM roots and rhizosphere in silver birch stands. Tartu, 2011.
46. **Ülle Marksoo.** Long-term unemployment and its regional disparities in Estonia. Tartu, 2011, 163 p.
47. **Hando Hain.** The role of voluntary certification in promoting sustainable natural resource use in transitional economies. Tartu, 2012, 180 p.
48. **Jüri-Ott Salm.** Emission of greenhouse gases CO_2, CH_4, and N_2O from Estonian transitional fens and ombrotrophic bogs: the impact of different land-use practices. Tartu, 2012, 125 p.
49. **Valentina Sagris.** Land Parcel Identification System conceptual model: development of geoinfo community conceptual model. Tartu, 2013, 161 p.
50. **Kristina Sohar.** Oak dendrochronology and climatic signal in Finland and the Baltic States. Tartu, 2013, 129 p.
51. **Riho Marja.** The relationships between farmland birds, land use and landscape structure in Northern Europe. Tartu, 2013, 134 p.
52. **Olle Järv.** Mobile phone based data in human travel behaviour studies: New insights from a longitudinal perspective. Tartu, 2013, 168 p.
53. **Sven-Erik Enno.** Thunderstorm and lightning climatology in the Baltic countries and in northern Europe. Tartu, 2014, 142 p.
54. **Kaupo Mändla.** Southern cyclones in northern Europe and their influence on climate variability. Tartu, 2014, 142 p.
55. **Riina Vaht.** The impact of oil shale mine water on hydrological pathways and regime in northeast Estonia. Tartu, 2014, 111 p.
56. **Jaanus Veemaa.** Reconsidering geography and power: policy ensembles, spatial knowledge, and the quest for consistent imagination. Tartu, 2014, 163 p.
57. **Kristi Anniste.** East-West migration in Europe: The case of Estonia after regaining independence. Tartu, 2014, 151 p.
58. **Piret Pungas-Kohv.** Between maintaining and sustaining heritage in landscape: The examples of Estonian mires and village swings. Tartu, 2015, 210 p.
59. **Mart Reimann.** Formation and assessment of landscape recreational values. Tartu, 2015, 127 p.
60. **Järvi Järveoja.** Fluxes of the greenhouse gases CO_2, CH_4 and N_2O from abandoned peat extraction areas: Impact of bioenergy crop cultivation and peatland restoration. Tartu, 2015, 171 p.
61. **Raili Torga.** The effects of elevated humidity, extreme weather conditions and clear-cut on greenhouse gas emissions in fast growing deciduous forests. Tartu, 2016, 128 p.
62. **Mari Nuga.** Soviet-era summerhouses On homes and planning in post-socialist suburbia. Tartu, 2016, 179 p.

63. **Age Poom.** Spatial aspects of the environmental load of consumption and mobility. Tartu, 2017, 141 p.
64. **Merle Muru.** GIS-based palaeogeographical reconstructions of the Baltic Sea shores in Estonia and adjoining areas during the Stone Age. Tartu, 2017, 132 p.
65. **Ülle Napa.** Heavy metals in Estonian coniferous forests. Tartu, 2017, 129 p.
66. **Liisi Jakobson.** Mutual effects of wind speed, air temperature and sea ice concentration in the Arctic and their teleconnections with climate variability in the eastern Baltic Sea region. Tartu, 2018, 118 p.
67. **Tanel Tamm.** Use of local statistics in remote sensing of grasslands and forests. Tartu, 2018, 106 p.
68. **Enel Pungas.** Differences in Migration Intentions by Ethnicity and Education: The Case of Estonia. Tartu, 2018, 142 p.
69. **Kadi Mägi.** Ethnic residential segregation and integration of the Russian-speaking population in Estonia. Tartu, 2018, 173 p.
70. **Kiira Mõisja.** Thematic accuracy and completeness of topographic maps. Tartu, 2018, 112 p.
71. **Kristiina Kukk.** Understanding the vicious circle of segregation: The role of leisure time activities. Tartu, 2019, 143 p.
72. **Kaie Kriiska.** Variation in annual carbon fluxes affecting the soil organic carbon pool and the dynamics of decomposition in hemiboreal coniferous forests. Tartu, 2019, 146 p.
73. **Pille Metspalu.** The changing role of the planner. Implications of creative pragmatism in Estonian spatial planning. Tartu, 2019, 128 p.
74. **Janika Raun.** Mobile positioning data for tourism destination studies and statistics. Tartu, 2020, 153 p.
75. **Birgit Viru.** Snow cover dynamics and its impact on greenhouse gas fluxes in drained peatlands in Estonia. Tartu, 2020, 123 p.
76. **Iuliia Burdun.** Improving groundwater table monitoring for Northern Hemisphere peatlands using optical and thermal satellite data. Tartu, 2020, 162 p.
77. **Ingmar Pastak.** Gentrification and displacement of long-term residents in post-industrial neighbourhoods of Tallinn. Tartu, 2021, 141 p.
78. **Veronika Mooses.** Towards a more comprehensive understanding of ethnic segregation: activity space and the vicious circle of segregation. Tartu, 2021, 161 p.
79. **Johanna Pirrus.** Contemporary Urban Policies and Planning Measures in Socialist-Era Large Housing Estates. Tartu, 2021, 142 p.
80. **Gert Veber.** Greenhouse gas fluxes in natural and drained peatlands: spatial and temporal dynamics. Tartu, 2021, 210 p.
81. **Anniki Puura.** Relationships between personal social networks and spatial mobility with mobile phone data. Tartu, 2021, 144 p.
82. **Alisa Krasnova.** Greenhouse gas fluxes in hemiboreal forest ecosystems. Tartu, 2022, 185 p.

83. **Tauri Tampuu.** Synthetic Aperture Radar Interferometry as a tool for monitoring the dynamics of peatland surface. Tartu, 2022, 166 p.
84. **Najmeh Mozaffaree Pour.** Urban Expansion in Estonia: Monitoring, Analysis, and Modeling. Tartu, 2022, 169 p.
85. **Bruno Montibeller**. Evaluating human-induced forest degradation in different biomes using spatial analysis of satellite-derived data. Tartu, 2022, 112 p.
86. **Holger Virro**. Geospatial data harmonization and machine learning for large-scale water quality modelling. Tartu, 2022, 138 p.
87. **Azadeh Rezapour**. The impact of climate change on fine root trait responses of deciduous and coniferous trees. Tartu, 2023, 108 p.
88. **Isaac Newton Kwasi Buo**. Multi-scale thermal Remote Sensing, Machine Learning, and Radiative Flux Modeling to Assess Urban Overheating. Tartu, 2023, 116 p.
89. **David Knapp**. The relationship between residential segregation, school segregation and family context. Tartu, 2024, 122 p.
90. **Reti Ranniku**. Impact of environmental conditions and soil microbiome on greenhouse gas fluxes from soil and tree stems in hemiboreal drained peatland forest. Tartu, 2024, 142 pp.